

# On the Variation of Fourier Parameters for Galactic and LMC Cepheids at Optical, Near-Infrared and Mid-Infrared Wavelengths

Anupam Bhardwaj<sup>1\*</sup>, Shashi M. Kanbur<sup>2</sup>, Harinder P. Singh<sup>1</sup>, Lucas M. Macri<sup>3</sup>,  
Chow-Choong Ngeow<sup>4</sup>

1. *Department of Physics & Astrophysics, University of Delhi, Delhi 110007, India.*

2. *State University of New York, Oswego, NY 13126, USA.*

3. *Mitchell Institute for Fundamental Physics & Astronomy, Department of Physics & Astronomy, Texas A&M University, College Station, TX 77843, USA*

4. *Graduate Institute of Astronomy, National Central University, Jhongli 32001, Taiwan*

Accepted 2014 December 15. Received 2014 December 15; in original form 2014 July 29

## ABSTRACT

We present a light curve analysis of fundamental-mode Galactic and Large Magellanic Cloud (LMC) Cepheids based on the Fourier decomposition technique. We have compiled light curve data for Galactic and LMC Cepheids in optical ( $VI$ ), near-infrared ( $JHK_s$ ) and mid-infrared (3.6 & 4.5- $\mu\text{m}$ ) bands from the literature and determined the variation of their Fourier parameters as a function of period and wavelength. We observed a decrease in Fourier amplitude parameters and an increase in Fourier phase parameters with increasing wavelengths at a given period. We also found a decrease in the skewness and acuteness parameters as a function of wavelength at a fixed period. We applied a binning method to analyze the progression of the mean Fourier parameters with period and wavelength. We found that for periods longer than about 20 days, the values of the Fourier amplitude parameters increase sharply for shorter wavelengths as compared to wavelengths longer than the  $J$ -band. We observed the variation of the Hertzsprung progression with wavelength. The central period of the Hertzsprung progression was found to increase with wavelength in the case of the Fourier amplitude parameters and decrease with increasing wavelength in the case of phase parameters. We also observed a small variation of the central period of the progression between the Galaxy and LMC, presumably related to metallicity effects. These results will provide useful constraints for stellar pulsation codes that incorporate stellar atmosphere models to produce Cepheid light curves in various bands.

**Key words:** stars: variables: Cepheids - (galaxies:) Magellanic Clouds.

## 1 INTRODUCTION

Cepheid variables are bright, population I periodic radial pulsators that exhibit regular light curves and obey a well known Period-Luminosity relation (Leavitt & Pickering 1912), that is an important tool in the extra-galactic distance scale. Fourier analysis methods have been used extensively to describe Cepheid light curve structure and its variation with period. In particular, the amplitude ratios ( $R_{21}$  and  $R_{31}$ ) and phase differences ( $\phi_{21}$  and  $\phi_{31}$ ) have been used to quantitatively describe the progression of Cepheid light curve shape with period (Simon 1977). The Fourier decom-

position method was further revived by Simon & Lee (1981), who used a sample of 57 Cepheids and discussed the variation of Fourier parameters with period. The sharp breaks in the progressions of Fourier parameters with period, occurring near 10 days, were attributed to the resonance  $P_2/P_0 = 0.5$ , in the normal mode spectrum (Simon & Schmidt 1976; Simon 1977; Simon & Lee 1981). Later, the method was used extensively by Simon & Teays (1982) to analyze the progressions of Fourier parameters and light curve structure of a large sample of field RR Lyrae stars. The light and velocity curves were Fourier decomposed to compare with theoretically modeled light curves (Simon & Davis 1983; Simon & Moffett 1985). Similar studies of the light curve structures of RR Lyrae variables were carried out by Simon

\* E-mail: anupam.bhardwaj@gmail.com

(1985); Kovacs, Shlosman & Buchler (1986). The Fourier phase parameter ( $\phi_{31}$ ) was used in empirical relations to determine the metallicity of fundamental mode RR Lyrae stars (Jurcsik & Kovacs 1996). The studies on theoretical light curves of Cepheid variables using the skewness and acuteness parameters together with the variation of Fourier parameters were carried out by Stellingwerf & Donohoe (1986, 1987); Bono, Marconi & Stellingwerf (2000). The central period of Hertzsprung progression was also determined using the Fourier parameters (Moskalik, Buchler & Marom 1992; Welch et al. 1997; Beaulieu 1998) and skewness/acuteness parameters (Bono, Marconi & Stellingwerf 2000). Other studies employing the Fourier decomposition technique to analyze the light curves of Cepheid variables, are Simon (1986); Antonello & Poretti (1986); Andreasen & Petersen (1987); Andreasen (1988); Simon (1988); Poretti (1994); Simon & Kanbur (1995); Stetson (1996); Welch et al. (1997); Beaulieu (1998).

Recent applications of this method include the reconstruction of Cepheid light curves with Fourier technique (Ngeow et al. 2003), and classification of variable star light curves based on Fourier parameters and Principal Component Analysis (PCA, Deb & Singh 2009). Most of the recent studies on Fourier decomposition involve the determination of physical parameters like absolute magnitude, metallicity, effective temperature, luminosity for RR Lyrae variables (Deb & Singh 2010; Nemec et al. 2011). The Fourier decomposition technique has been further extended to describe the chemical and structural properties of the LMC (Deb & Singh 2014).

In this work, we analyze the light curves of fundamental-mode Galactic and LMC Cepheids in multiple bands using Fourier decomposition techniques. In Section 2, we provide a brief description of the application of the Fourier decomposition method. In Section 3, we discuss the Galactic and LMC Cepheid light curve data compiled from the literature for optical, near-infrared and mid-infrared wavelengths. In Section 4, we describe the application of Fourier decomposition to Galactic and LMC Cepheid light curves. Further, we discuss the variation of Fourier parameters with period in each band separately. In Section 5, we compare the Fourier parameters in multiple bands and comment on their progression with period and wavelength. We also discuss the variation of mean Fourier parameters together with skewness and acuteness parameters as a function of wavelength at a given period. In Section 6, we summarize the variation of the central period of the Hertzsprung progression with wavelength for each Fourier parameter in the Galaxy and LMC. A discussion on our results and important conclusions arising from this study are presented in Section 7.

Our results will provide important constraints for stellar pulsation codes that incorporate stellar atmosphere models to produce wavelength-dependent theoretical Cepheid light curves.

## 2 FOURIER DECOMPOSITION TECHNIQUE

Fourier decomposition is a robust method to study the light curves of variable stars. This method was revived and refined by Simon & Lee (1981) in its modern form. They described how the lower order Fourier coefficients can com-

pletely describe the structure of the light curve. The Fourier coefficients and Fourier parameters are now widely used to derive empirical relations to determine physical parameters of variable stars, in particular for fundamental mode RR Lyrae stars.

In this study we have used a sine Fourier series to fit the multi-band light curves of Galactic and LMC Cepheids,

$$m(t) = m_0 + \sum_{i=1}^N A_i \sin(i\omega(t - t_0) + \phi_i), \quad (1)$$

where  $m(t)$  is the observed magnitude,  $m_0$  is the mean magnitude from the Fourier fit,  $t$  is the time of observation,  $\omega = 2\pi/P$  is the angular frequency and  $t_0$  corresponds to the epoch of maximum brightness. In this study, we have taken  $t_0$  as the time of minimum magnitude from the light curve data for each Cepheid, which is used to obtain a phased light curve that has maximum light at phase zero.  $A_i$  and  $\phi_i$  are amplitude and phase coefficients respectively. Since the period  $P$  is known, the light curves are phased using

$$x = \text{frac} \left( \frac{t - t_0}{P} \right).$$

Since the values of  $x$  range from 0 to 1, corresponding to a full cycle of pulsation, equation (1) can be written as:

$$m = m_0 + \sum_{i=1}^N A_i \sin(2\pi ix + \phi_i). \quad (2)$$

Here,  $N$  is the optimum order of fit, which is generally chosen depending on the size of least square residuals. Furthermore, coefficients  $A_1 \dots A_N$  and  $\phi_1 \dots \phi_N$  are extracted from the fit to give Fourier parameters,

$$R_{i1} = \frac{A_i}{A_1}; \phi_{i1} = \phi_i - i\phi_1, \quad (3)$$

where  $i > 1$ . The  $\phi_{i1}$  are generally adjusted to lie between 0 and  $2\pi$ . The errors in the derived Fourier parameters are determined using the propagation of errors in the coefficients (Deb & Singh 2010).

## 3 THE DATA

The data selected for present analysis is described in Table 1. A brief description of each catalogue/source used is presented in the following subsections.

### 3.1 Optical Wavelengths

#### 3.1.1 Galactic Cepheids

The light curve data for Galactic Cepheids in the Johnson  $V$ - and Kron-Cousins  $I$ -bands were extracted from the catalogue of Berdnikov (2008). This catalogue gathers photoelectric observations of Galactic Cepheids made between 1986 and 2004 by Berdnikov and his collaborators in a series of papers (Berdnikov 1987, 1992; Berdnikov & Yakubov 1993; Berdnikov & Vozyakova 1995; Berdnikov, Ignatova & Pastukhova 1998; Berdnikov & Turner 2001, 2004a,b). Our analysis makes

**Table 1.** The Galactic and LMC Cepheid multi-wavelength light curve data selected for the present analysis.

Band	Galaxy		LMC	
	No. of stars	References	No. of stars	References
<i>V</i>	447	Berdnikov (2008)	1832	Soszynski et al. (2008); Ulaczyk et al. (2013)
<i>I</i>	351	-	1844	-
<i>J</i>	186	Welch et al. (1984); Laney & Stobie (1992); Barnes et al. (1997); Monson & Pierce (2011)	474	Macri et al. (2014); Persson et al. (2004)
<i>H</i>	186	-	532	-
<i>K<sub>s</sub></i>	186	-	488	-
3.6- $\mu\text{m}$	37	Monson et al. (2012)	84	Scowcroft et al. (2011)
4.5- $\mu\text{m}$	37	-	84	-

use of 447 and 351 Galactic Cepheids with data in the *V*- and *I*-bands, respectively. Since this catalogue is compiled from a series of observations carried out over two decades, the number of data points for each star ranges from 20 to nearly 400. The periods of the variables were extracted from the database of Galactic Classical Cepheids (Ferne et al. 1995).

### 3.1.2 LMC Cepheids

The light curve data for LMC Cepheids in the *V*- and *I*-bands were taken from the third phase of the Optical Gravitational Lensing Experiment (OGLE-III) survey (Soszynski et al. 2008). The observations were carried out using a dedicated 1.3-m telescope at the Las Campanas Observatory, Chile. Our analysis makes use of 1806 and 1818 light curves in the *V*- and *I*-bands, respectively. The light curves are fairly well sampled with a large number of data points in *I*-band, and covering nearly full phase in both optical bands. We also make use of the period and initial epoch provided in this database to Fourier fit the light curves.

We also extracted the light curve data in the *V*- and *I*-bands for 26 long period Cepheids from OGLE-III Shallow Survey in the LMC (Ulaczyk et al. 2013). The photometric data for these Cepheids were also collected using the 1.3-m Warsaw Telescope located at Las Campanas Observatory. Since the photometric system is exactly similar in both the surveys (Soszynski et al. (2008) & Ulaczyk et al. (2013)), we increase our sample to have 1832 Cepheids in *V*-band and 1844 Cepheids in *I*-band.

## 3.2 Near-Infrared Wavelengths

### 3.2.1 Galactic Cepheids

We compiled photometric data for 186 Galactic Cepheids in the *JHK<sub>s</sub>* bands with full phase coverage using several sources in the literature (Welch et al. 1984; Laney & Stobie 1992; Barnes et al. 1997; Monson & Pierce 2011). The light

curves taken from Monson & Pierce (2011) for 129 Galactic Cepheids were obtained during a span of 10 months in 2008 using the BIRCAM instrument at the 0.6-m telescope of the University of Wyoming Red Buttes Observatory (RBO). These light curves have an average of 22 observations per star, providing reasonable phase coverage. We included 41 light curves from Laney & Stobie (1992) that were obtained between 1982 to 1990 at the Sutherland observing station of South African Astronomical Observatory. Most of the observations were carried out using the 0.75-m telescope and the Mark II infrared photometer and the remaining observations were made using the 1.9-m telescope and the Mark III infrared photometer. These light curves have 31 data points per star. We also made use of 8 light curves from Barnes et al. (1997), obtained at the 1.3-m telescope at Kitt Peak National Observatory using the OTTO and SQUID instruments. Lastly, we incorporated 8 variables from Welch et al. (1984) that were obtained using the 1-m Swope telescope at Las Campanas Observation, Chile and the 0.6-m telescope at Mount Wilson using the 0.6-m reflector.

Since these near-infrared light curve data were obtained by the various authors using different photometric systems, we transformed them into the 2MASS system using the transformations provided as part of their all-sky data release<sup>1</sup>.

### 3.2.2 LMC Cepheids

Our analysis made use of combined LMC near-infrared light curve data for 474, 532 and 488 Cepheids in *J*, *H* and *K<sub>s</sub>*, respectively, from the two sources listed below.

We used the light curve data from Macri et al. (2014), who carried out a *JHK<sub>s</sub>* survey of the central  $\sim 18^\circ$  of the LMC using the CPAPIR camera at the Cerro Tololo Inter-American Observatory (CTIO) 1.5-m telescope, operated as part of the SMARTS consortium. The variables, originally

<sup>1</sup> [http://www.ipac.caltech.edu/2mass/releases/allsky/doc/sec6\\_4b.html](http://www.ipac.caltech.edu/2mass/releases/allsky/doc/sec6_4b.html)

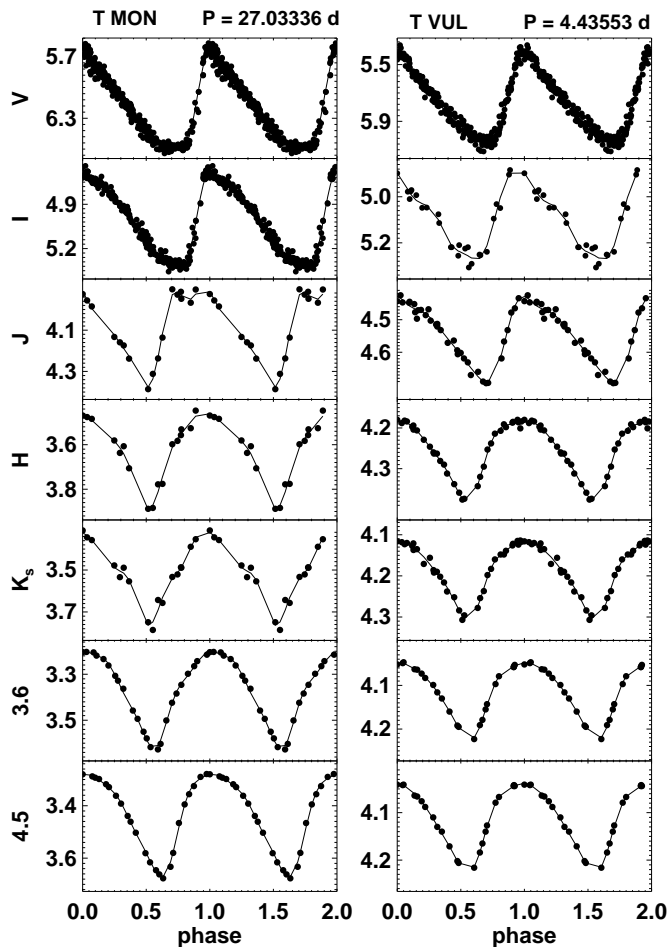


**Figure 1.** Examples of the Fourier-fitted light curves of two Galactic Cepheids in multiple bands. The star ID is given at the top of each panel.

identified by OGLE-III (Soszynski et al. 2008) range in period from 1 to 37 days, with an average number of 16 phase points per object. The observations were calibrated by the authors into the 2MASS system. We used 384, 442, 398 light curves in  $J$ ,  $H$  &  $K_s$ , respectively.

We have also used the  $JHK_s$  data for 90 Cepheids in the LMC from Persson et al. (2004). These observations were carried out with the 1-m Swope and 2.5-m duPont telescopes at Las Campanas Observatory between 1993 to 1997. These stars have periods in the range of 2 to 134 days and an average of 22 observations per band. These observations were reported using the LCO photometric system, and were transformed into the 2MASS system using the previously referenced relations.

### 3.3 Mid-Infrared Wavelengths

We used the 3.6 and 4.5- $\mu\text{m}$  light curves of 37 Galactic and 84 LMC Cepheids obtained by Monson et al. (2012) and Scowcroft et al. (2011), respectively, using *Spitzer* and IRAC channels 1 & 2. The variables range in period from 4 to 70

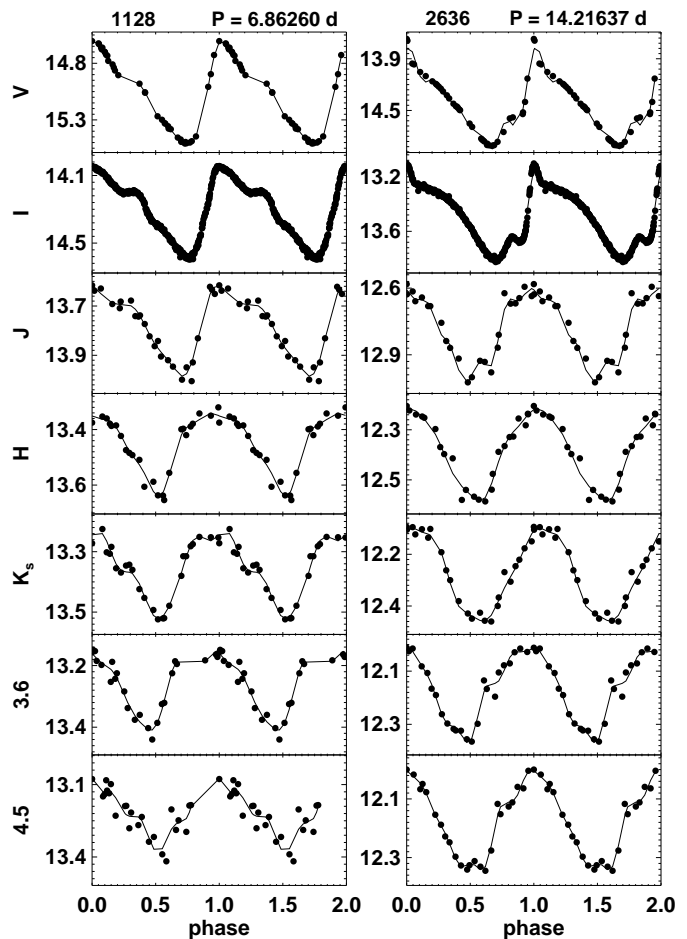


**Figure 2.** Same as Figure 1, but for two LMC Cepheids. Star ID's consisting of 4 numbers are based on the OGLE-III catalog. These variables are identified as HV2337 & HV1006 in Persson et al. (2004) and Scowcroft et al. (2011)

days for the Milky Way and 6 to 140 days for the LMC, and were observed at 24 phase points from 2009 to 2011.

## 4 FOURIER ANALYSIS OF GALACTIC AND LMC CEPHEIDS

We applied the Fourier decomposition method discussed in Section 2 individually to each Galactic and LMC Cepheid light curve, analyzing each bandpass separately. We implemented equation (2) using the IDL MPCURVEFIT routine, varying the order of the fit in each band from 4 to 8. The optimum order of fit ( $N$ ) was determined using Baart's condition, depending on the residuals for each star (Baart 1982; Deb & Singh 2009). The resulting Fourier coefficients were used to calculate Fourier parameters using equation (3). Fourier-fitted light curves for two Galactic and two LMC Cepheids are shown in Fig. 1 and 2, respectively. The Fourier parameters for all variables in all bands are presented in Tables 2 and 3 for Galactic and LMC Cepheids, respectively.

**Table 2.** Fourier parameters obtained using a sine series Fourier fit to the Galactic Cepheid light curves in multi-bands.

Star ID	$\log(P)$	$t_0$ (JD)	$N$	$S_k(V)$	$A_c(V)$	$A_1(V)$ $\sigma_{A_1(V)}$	$\phi_1(V)$ $\sigma_{\phi_1(V)}$	$R_{21}(V)$ $\sigma_{R_{21}(V)}$	$R_{31}(V)$ $\sigma_{R_{31}(V)}$	$\phi_{21}(V)$ $\sigma_{\phi_{21}(V)}$	$\phi_{31}(V)$ $\sigma_{\phi_{31}(V)}$
AA GEM	1.05317	2450327.50	4	1.15054	1.29358	0.28474 0.00018	4.54609 0.00062	0.04594 0.00063	0.14852 0.00064	1.15955 0.01319	3.44948 0.00463
AA MON	0.59529	2449805.60	4	3.44444	1.51889	0.28038 0.00091	4.04757 0.00259	0.39447 0.00158	0.22337 0.00326	2.56312 0.01115	5.53655 0.01508
Star ID	$\log(P)$	$t_0$ (JD)	$N$	$S_k(I)$	$A_c(I)$	$A_1(I)$ $\sigma_{A_1(I)}$	$\phi_1(I)$ $\sigma_{\phi_1(I)}$	$R_{21}(I)$ $\sigma_{R_{21}(I)}$	$R_{31}(I)$ $\sigma_{R_{31}(I)}$	$\phi_{21}(I)$ $\sigma_{\phi_{21}(I)}$	$\phi_{31}(I)$ $\sigma_{\phi_{31}(I)}$
AA MON	0.59529	2449809.60	4	1.98507	1.37530	0.16641 0.00092	3.92683 0.00427	0.42473 0.00311	0.25341 0.00559	3.18826 0.01736	6.21661 0.02306
AA SER	1.23404	2451255.60	4	1.46914	1.29885	0.25341 0.00015	4.37060 0.00062	0.20465 0.00064	0.12324 0.00060	2.91294 0.00313	5.09847 0.00538
Star ID	$\log(P)$	$t_0$ (JD)	$N$	$S_k(J)$	$A_c(J)$	$A_1(J)$ $\sigma_{A_1(J)}$	$\phi_1(J)$ $\sigma_{\phi_1(J)}$	$R_{21}(J)$ $\sigma_{R_{21}(J)}$	$R_{31}(J)$ $\sigma_{R_{31}(J)}$	$\phi_{21}(J)$ $\sigma_{\phi_{21}(J)}$	$\phi_{31}(J)$ $\sigma_{\phi_{31}(J)}$
AA GEM	1.05320	2454487.90	4	1.30415	0.93050	0.09333 0.00420	4.35333 0.04400	0.11786 0.04489	0.11175 0.04571	3.08027 0.39112	5.07397 0.41752
AA MON	0.59530	2454523.80	5	1.73224	0.62075	0.13759 0.01007	3.97621 0.07183	0.30773 0.04312	0.09935 0.06271	3.68045 0.28293	0.61230 0.61763
Star ID	$\log(P)$	$t_0$ (JD)	$N$	$S_k(H)$	$A_c(H)$	$A_1(H)$ $\sigma_{A_1(H)}$	$\phi_1(H)$ $\sigma_{\phi_1(H)}$	$R_{21}(H)$ $\sigma_{R_{21}(H)}$	$R_{31}(H)$ $\sigma_{R_{31}(H)}$	$\phi_{21}(H)$ $\sigma_{\phi_{21}(H)}$	$\phi_{31}(H)$ $\sigma_{\phi_{31}(H)}$
AA GEM	1.05320	2454579.70	4	1.28833	0.81818	0.10383 0.00385	4.43851 0.03727	0.11384 0.03741	0.02841 0.03854	4.07990 0.33727	4.47053 1.28316
AA MON	0.59530	2454516.80	4	0.75439	0.32450	0.10127 0.00682	5.12493 0.06674	0.34107 0.05294	0.25289 0.06307	4.43058 0.25083	2.00580 0.33918
Star ID	$\log(P)$	$t_0$ (JD)	$N$	$S_k(K_s)$	$A_c(K_s)$	$A_1(K_s)$ $\sigma_{A_1(K_s)}$	$\phi_1(K_s)$ $\sigma_{\phi_1(K_s)}$	$R_{21}(K_s)$ $\sigma_{R_{21}(K_s)}$	$R_{31}(K_s)$ $\sigma_{R_{31}(K_s)}$	$\phi_{21}(K_s)$ $\sigma_{\phi_{21}(K_s)}$	$\phi_{31}(K_s)$ $\sigma_{\phi_{31}(K_s)}$
AA GEM	1.05320	2454579.70	4	0.79533	0.72712	0.11488 0.00593	0.12856 0.05171	0.12718 0.05281	0.03795 0.05453	5.01138 0.41751	3.95453 1.31282
AA MON	0.59530	2454492.80	5	1.55102	0.35318	0.09332 0.01086	5.16933 0.14467	0.39145 0.08171	0.24175 0.11754	4.52406 0.45003	2.11436 0.60624
Star ID	$\log(P)$	$t_0$ (JD)	$N$	$S_k(3.6)$	$A_c(3.6)$	$A_1(3.6)$ $\sigma_{A_1(3.6)}$	$\phi_1(3.6)$ $\sigma_{\phi_1(3.6)}$	$R_{21}(3.6)$ $\sigma_{R_{21}(3.6)}$	$R_{31}(3.6)$ $\sigma_{R_{31}(3.6)}$	$\phi_{21}(3.6)$ $\sigma_{\phi_{21}(3.6)}$	$\phi_{31}(3.6)$ $\sigma_{\phi_{31}(3.6)}$
BETA DOR	0.99300	2455185.614	4	0.66113	0.91939	0.09493 0.00516	4.81700 0.04490	0.12778 0.05271	0.02570 0.05111	5.97377 0.41966	0.57282 1.97951
CD CYG	1.23200	2455370.893	4	1.25734	0.63132	0.18164 0.00368	4.86587 0.01584	0.17023 0.01920	0.06485 0.01876	4.51443 0.10726	2.56212 0.26134
Star ID	$\log(P)$	$t_0$ (JD)	$N$	$S_k(4.5)$	$A_c(4.5)$	$A_1(4.5)$ $\sigma_{A_1(4.5)}$	$\phi_1(4.5)$ $\sigma_{\phi_1(4.5)}$	$R_{21}(4.5)$ $\sigma_{R_{21}(4.5)}$	$R_{31}(4.5)$ $\sigma_{R_{31}(4.5)}$	$\phi_{21}(4.5)$ $\sigma_{\phi_{21}(4.5)}$	$\phi_{31}(4.5)$ $\sigma_{\phi_{31}(4.5)}$
BETA DOR	0.99300	2455176.550	4	0.66667	0.98020	0.09632 0.00296	5.05796 0.02814	0.08150 0.02721	0.06209 0.02654	0.02167 0.40379	5.38938 0.52805
CD CYG	1.23200	2455361.685	4	1.31481	0.71821	0.18603 0.00160	4.46042 0.00924	0.16540 0.00893	0.02301 0.01038	4.11389 0.06042	1.83127 0.35669

**Notes:** This table is available entirely in a machine-readable form in the online journal.

In all the figures presented in our paper, the values of the Fourier phase parameter  $\phi_{31}$ , obtained using a sine series, were converted into cosine series by adding a value of  $\pi$  to those given in Table 2 and 3 (Deb & Singh 2014).

#### 4.1 Optical Bands

We have determined the Fourier parameters ( $R_{21}$ ,  $R_{31}$ ,  $\phi_{21}$  &  $\phi_{31}$ ) of one of the largest samples of Galactic Cepheids at optical wavelengths, with 447 objects in  $V$  and 351 in  $I$ . These are shown in the top two rows of Fig. 3 as a function of  $\log(P)$ .

The Hertzsprung progression (hereafter HP), indicated



**Table 3.** Fourier parameters obtained using a sine series Fourier fit to the LMC Cepheid light curves in multi-bands. The Star ID's are from corresponding catalogues listed in Table 1 for each band.

Star ID	$\log(P)$	$t_0$ (JD)	$N$	$S_k(V)$	$A_c(V)$	$A_1(V)$ $\sigma_{A_1(V)}$	$\phi_1(V)$ $\sigma_{\phi_1(V)}$	$R_{21}(V)$ $\sigma_{R_{21}(V)}$	$R_{31}(V)$ $\sigma_{R_{31}(V)}$	$\phi_{21}(V)$ $\sigma_{\phi_{21}(V)}$	$\phi_{31}(V)$ $\sigma_{\phi_{31}(V)}$
0002	0.49389	2452171.239	4	2.44828	1.45700	0.19118 0.00175	4.19231 0.00844	0.33591 0.00951	0.12517 0.00860	2.66724 0.03024	5.50564 0.07721
0005	0.74912	2452171.781	4	2.95257	1.33100	0.34500 0.00104	3.97419 0.00303	0.45217 0.00328	0.16609 0.00286	3.03606 0.00910	5.91411 0.02181
Star ID	$\log(P)$	$t_0$ (JD)	$N$	$S_k(I)$	$A_c(I)$	$A_1(I)$ $\sigma_{A_1(I)}$	$\phi_1(I)$ $\sigma_{\phi_1(I)}$	$R_{21}(I)$ $\sigma_{R_{21}(I)}$	$R_{31}(I)$ $\sigma_{R_{31}(I)}$	$\phi_{21}(I)$ $\sigma_{\phi_{21}(I)}$	$\phi_{31}(I)$ $\sigma_{\phi_{31}(I)}$
0002	0.49389	2452171.239	4	2.17460	1.00803	0.11220 0.00051	4.11196 0.00470	0.29546 0.00474	0.10232 0.00457	3.14967 0.01856	6.16518 0.04814
0005	0.74912	2452171.781	8	3.14938	0.77305	0.20866 0.00044	3.84936 0.00222	0.43113 0.00234	0.16673 0.00218	3.40130 0.00670	0.25359 0.01464
Star ID	$\log(P)$	$t_0$ (JD)	$N$	$S_k(J)$	$A_c(J)$	$A_1(J)$ $\sigma_{A_1(J)}$	$\phi_1(J)$ $\sigma_{\phi_1(J)}$	$R_{21}(J)$ $\sigma_{R_{21}(J)}$	$R_{31}(J)$ $\sigma_{R_{31}(J)}$	$\phi_{21}(J)$ $\sigma_{\phi_{21}(J)}$	$\phi_{31}(J)$ $\sigma_{\phi_{31}(J)}$
0504	1.15812	2454438.279	4	1.51889	0.76056	0.24890 0.01604	4.33626 0.07310	0.13427 0.10346	0.11539 0.09234	3.26927 0.24731	1.21061 0.53270
0519	0.22527	2454422.182	6	0.92678	0.68350	0.22571 0.01811	3.81431 0.05389	0.28187 0.09476	0.16313 0.07209	3.91709 0.25880	1.58920 0.62753
Star ID	$\log(P)$	$t_0$ (JD)	$N$	$S_k(H)$	$A_c(H)$	$A_1(H)$ $\sigma_{A_1(H)}$	$\phi_1(H)$ $\sigma_{\phi_1(H)}$	$R_{21}(H)$ $\sigma_{R_{21}(H)}$	$R_{31}(H)$ $\sigma_{R_{31}(H)}$	$\phi_{21}(H)$ $\sigma_{\phi_{21}(H)}$	$\phi_{31}(H)$ $\sigma_{\phi_{31}(H)}$
0494	0.43568	2454046.364	5	0.17509	0.16279	0.17578 0.06525	6.10606 0.51883	1.53163 0.80457	1.06559 0.59504	0.32741 1.03915	5.88143 1.56241
0539	0.53844	2454426.226	4	0.77620	1.19298	0.21535 0.05844	3.32530 0.13329	0.34878 0.19470	0.35607 0.16559	6.18024 0.57905	2.34390 0.48191
Star ID	$\log(P)$	$t_0$ (JD)	$N$	$S_k(K_s)$	$A_c(K_s)$	$A_1(K_s)$ $\sigma_{A_1(K_s)}$	$\phi_1(K_s)$ $\sigma_{\phi_1(K_s)}$	$R_{21}(K_s)$ $\sigma_{R_{21}(K_s)}$	$R_{31}(K_s)$ $\sigma_{R_{31}(K_s)}$	$\phi_{21}(K_s)$ $\sigma_{\phi_{21}(K_s)}$	$\phi_{31}(K_s)$ $\sigma_{\phi_{31}(K_s)}$
0499	0.94601	2454107.035	4	0.97239	0.63132	0.10926 0.01208	4.74642 0.15320	0.17893 0.13889	0.13381 0.13772	4.95483 1.02475	2.32688 1.13511
0504	1.15812	2454426.228	6	0.67504	3.34783	0.14147 0.02404	4.55604 0.71908	0.29816 0.22381	0.43543 0.51429	5.49006 3.26315	3.30983 2.84190
Star ID	$\log(P)$	$t_0$ (JD)	$N$	$S_k(3.6)$	$A_c(3.6)$	$A_1(3.6)$ $\sigma_{A_1(3.6)}$	$\phi_1(3.6)$ $\sigma_{\phi_1(3.6)}$	$R_{21}(3.6)$ $\sigma_{R_{21}(3.6)}$	$R_{31}(3.6)$ $\sigma_{R_{31}(3.6)}$	$\phi_{21}(3.6)$ $\sigma_{\phi_{21}(3.6)}$	$\phi_{31}(3.6)$ $\sigma_{\phi_{31}(3.6)}$
HV1002	1.48390	2455153.441	4	0.91571	0.45985	0.20495 0.00305	4.66968 0.01473	0.22986 0.01508	0.12179 0.01548	4.64503 0.07240	3.12137 0.12744
HV1003	1.38630	2455144.947	4	0.95312	0.47929	0.15681 0.00333	4.82964 0.02091	0.21230 0.02109	0.14030 0.02088	4.93681 0.11005	2.83612 0.16887
Star ID	$\log(P)$	$t_0$ (JD)	$N$	$S_k(4.5)$	$A_c(4.5)$	$A_1(4.5)$ $\sigma_{A_1(4.5)}$	$\phi_1(4.5)$ $\sigma_{\phi_1(4.5)}$	$R_{21}(4.5)$ $\sigma_{R_{21}(4.5)}$	$R_{31}(4.5)$ $\sigma_{R_{31}(4.5)}$	$\phi_{21}(4.5)$ $\sigma_{\phi_{21}(4.5)}$	$\phi_{31}(4.5)$ $\sigma_{\phi_{31}(4.5)}$
HV1002	1.48390	2455152.041	4	1.33645	0.50830	0.21650 0.00330	4.63455 0.01493	0.22088 0.01534	0.13594 0.01465	4.21154 0.07610	2.92194 0.12536
HV1003	1.38630	2455142.933	4	1.18818	0.60256	0.16166 0.00364	4.58925 0.02225	0.18291 0.02198	0.17568 0.02219	4.63619 0.13488	2.19634 0.14987

**Notes:** This table is available entirely in a machine-readable form in the online journal. Star ID's consisting of 4 numbers are based on the OGLE-III catalog.

by a sharp dip or change in the way the Fourier parameters change with period, is clearly observed for  $R_{21}$ ,  $\phi_{21}$  &  $\phi_{31}$  in the vicinity of  $\log(P) = 1.0$ . The center of this HP seems to be located at slightly shorter period.  $R_{31}$  exhibits a flatter minimum that extends over a couple of days in the vicinity of  $\log(P) = 1.0$ . The uncertainties in the Fourier parameters

are very small, given the fairly good phase coverage and number of data points in the light curves.

The top two rows of Fig. 4 show the corresponding analysis for OGLE-III LMC Cepheids in  $V$ - and  $I$ -bands. These light curves have excellent sampling and full phase coverage, thereby yielding very well determined Fourier param-

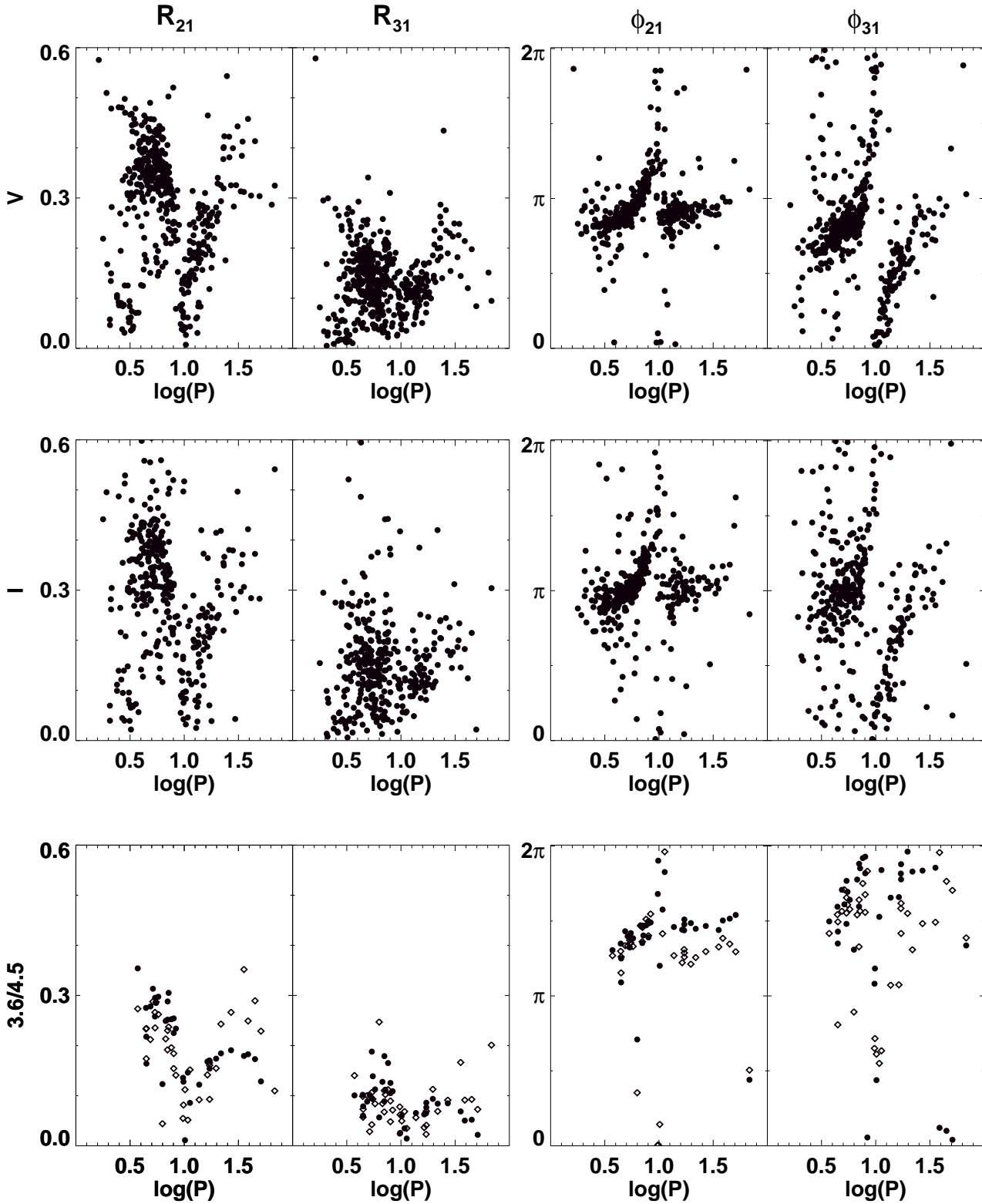


**Figure 3.** Galactic Cepheid Fourier parameters for the V (top row), I (middle row) and mid-infrared (bottom row) bands. In the mid-infrared panels, circles and diamonds represent 3.6 and 4.5  $\mu\text{m}$  data, respectively. The first two columns show Fourier amplitude parameters ( $R_{21}$  &  $R_{31}$ ) while the last two represent Fourier phase parameters ( $\phi_{21}$  &  $\phi_{31}$ ).

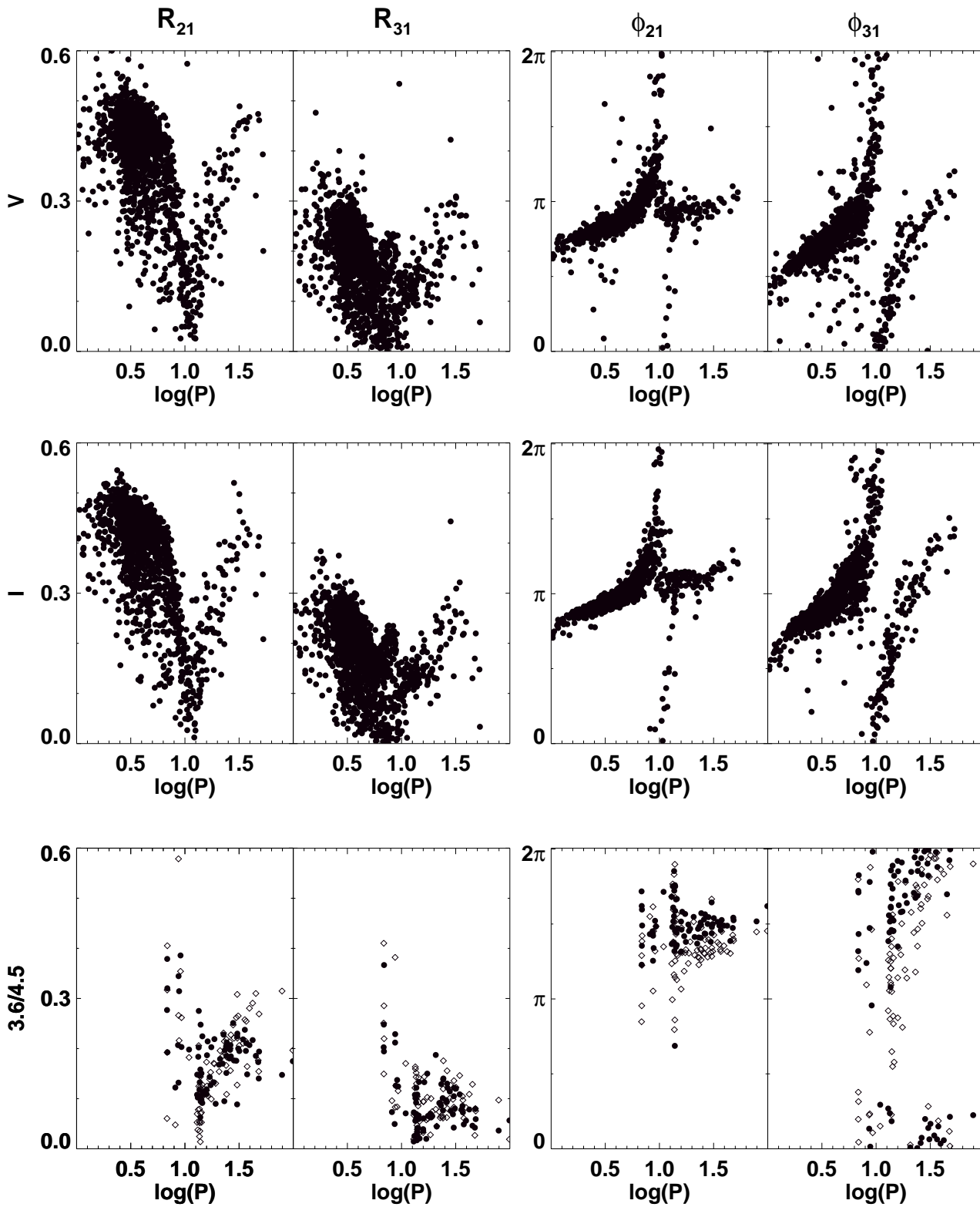


Figure 4. LMC Cepheid Fourier parameters, presented in the same manner as Fig. 3.



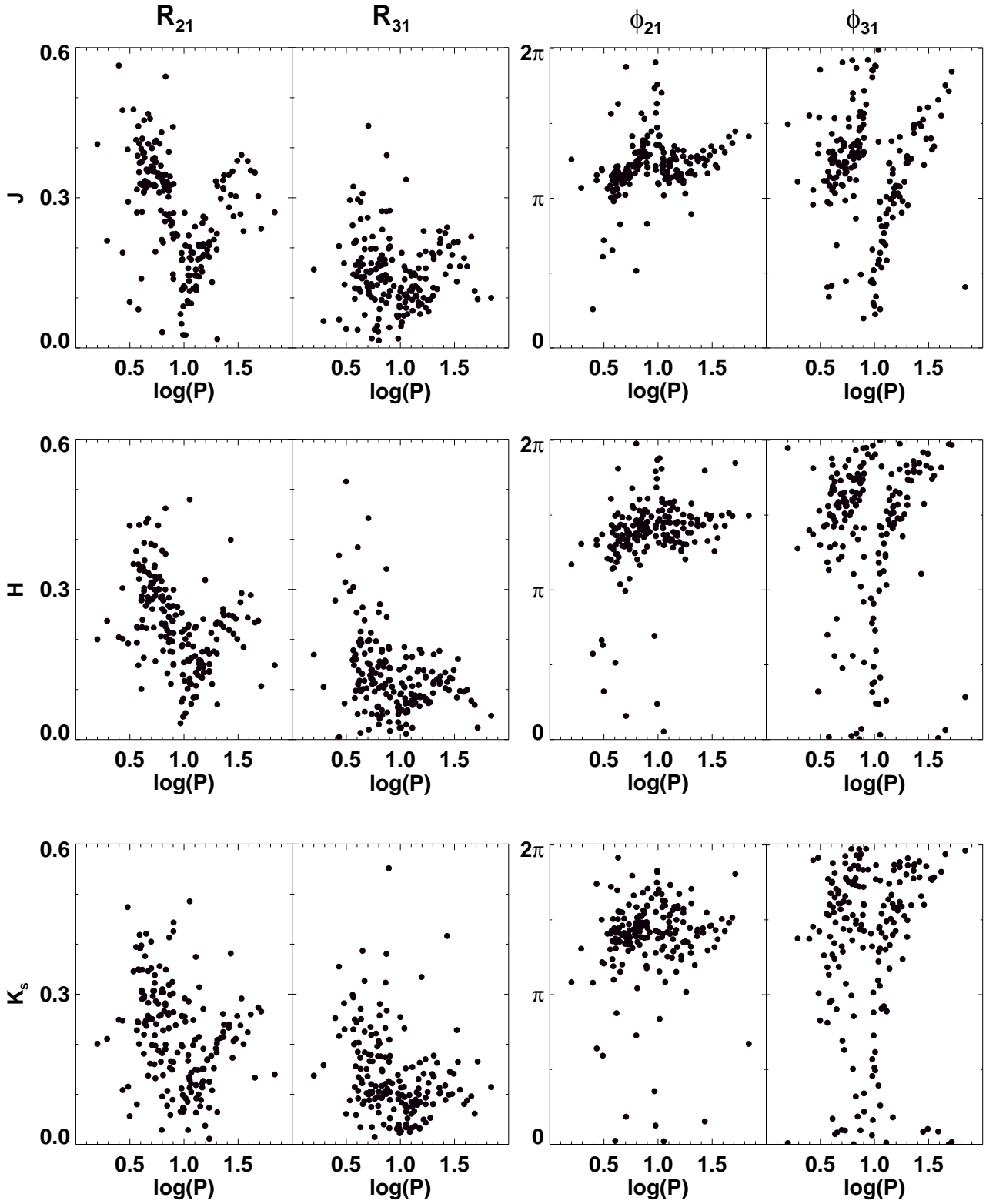


Figure 5. Galactic Cepheid Fourier parameters for the J (top row), H (middle row) and  $K_s$  (bottom row) bands, arranged in the column order as Fig. 3.

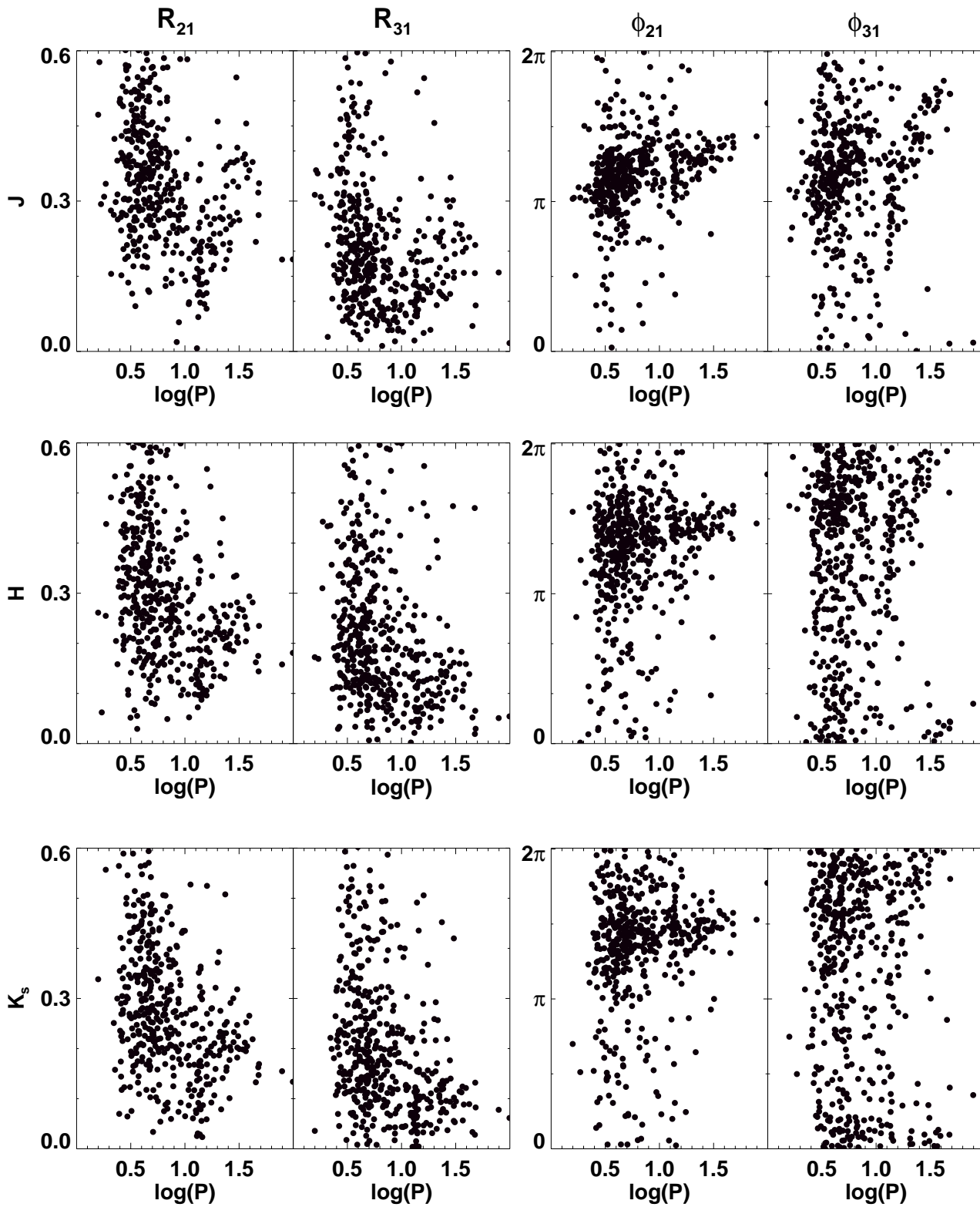
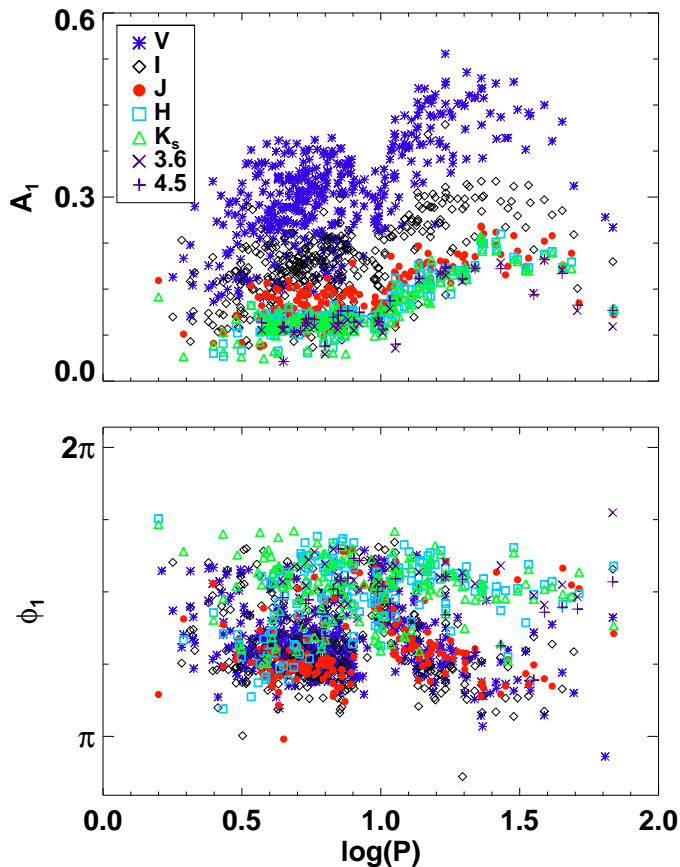


Figure 6. LMC Cepheid Fourier parameters, presented in the same manner as Fig. 5.



**Figure 7.** Variation of Fourier amplitude ( $A_1$ ) and phase ( $\phi_1$ ) coefficients for Galactic Cepheids in multiple bands.

ters that show clear patterns as discussed by Soszynski et al. (2008) & Ulaczyk et al. (2013) in their data release papers.

#### 4.2 Near-Infrared Bands

Fig. 5 presents the Fourier parameters for 186 Galactic Cepheids that presently have full phase coverage. The HP is clearly observed for all parameters in the vicinity of  $\log(P) = 1.0$ . We also noticed a more gradual increase of  $\phi_{31}$  for  $\log(P) > 1.0$  with increasing wavelength. Since the near-infrared data have a lower number of epochs and poorer phase coverage, the errors in the parameters are larger than at optical bands. The  $J$ -band parameters are the best determined ones, with increasing scatter at  $H$  and  $K_s$ .

Fig. 6 presents the corresponding results for the near-infrared LMC data, including the first-ever Fourier analysis of the light curves from Macri et al. (2014). Since these light curves are not as well sampled as their optical counterparts, we observe more scatter in the Fourier parameters. The better-sampled light curves from Persson et al. (2004), which predominantly cover variables with  $\log(P) > 1.0$ , enable us to clearly see the HP in the  $J$ -band Fourier parameters, while the  $H$  and  $K_s$  panels exhibit greater scatter.

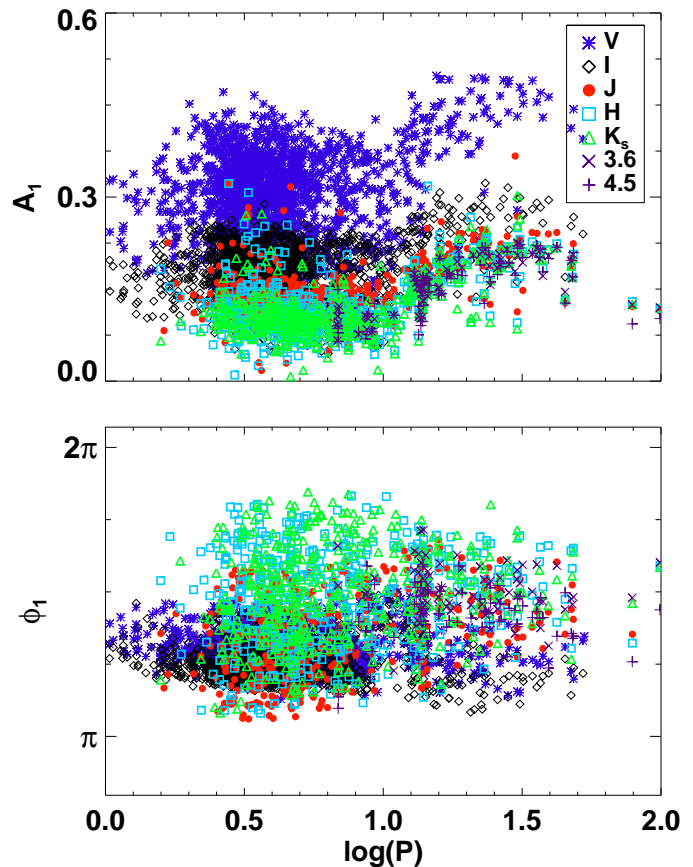


**Figure 8.** Same as Fig. 7, but for LMC Cepheids.

#### 4.3 Mid-Infrared Bands

The mid-infrared Fourier parameters for Galactic Cepheids are plotted in the bottom row of Fig. 3, showing for the first time the variation of light curve structure as a function of period at these wavelengths. Even with a smaller number of Cepheids in the sample, the HP is clearly visible for all Fourier parameters. The value of  $R_{21}$  displays an abrupt rise from  $\log(P) = 1.0$  to a maximum value of  $\log(P) = 1.5$  at  $4.5\text{-}\mu\text{m}$ , which is not seen at  $3.6\text{-}\mu\text{m}$ . Since these light curves have equal phase spacing and the same number of data points, the errors in the parameters are smaller than in their near-infrared counterparts.

The corresponding parameters for LMC Cepheids are displayed in the bottom row of Fig. 4. We observe similar patterns to those exhibited by the Galactic variables.

## 5 COMPARISON OF FOURIER PARAMETERS

### 5.1 Fourier amplitude and phase coefficient

We discuss the variation of the first harmonic of amplitude ( $A_1$ ) and first Fourier phase coefficient ( $\phi_1$ ) with period and wavelength. The plots are shown in Fig. 7 and 8, for Galactic and LMC Cepheids respectively. We removed the  $2\sigma$  outliers in these plots to make the progression visible. At a given

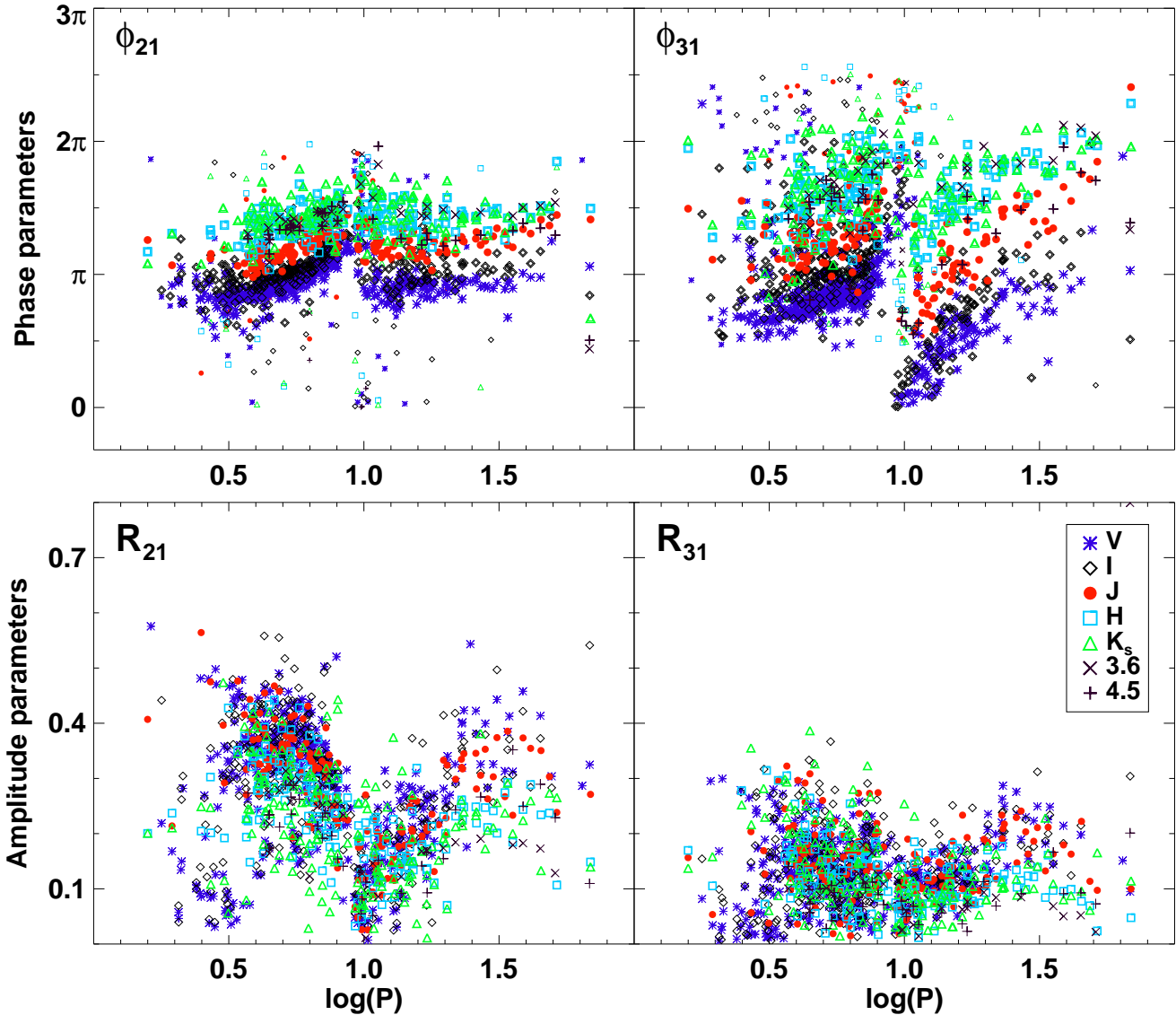


**Figure 9.** Fourier parameters plotted against  $\log(P)$  for Galactic Cepheids, in multiple bands. Some phase parameters have been shifted by  $2\pi$  for plotting purposes. The outliers in phase parameters for each band are shown using smaller symbols.

period, we observe a decrease in the value of  $A_1$  and an increase in  $\phi_1$  with increasing wavelength for both Galaxy and LMC. For  $1.0 < \log(P) < 1.5$ , we find a greater increase in the value of  $A_1$  and decrease in  $\phi_1$  at optical bands as compared to their infrared counterparts. Also, for  $\log(P) > 1.3$ , both coefficients show a very small variation and nearly a flat curve at infrared bands. A larger scatter in the value of  $\phi_1$  is observed for infrared bands.

We note that the variation of light curve amplitude is essentially similar to  $A_1$  but the variation of phase of maximum light (corresponding to  $t_0$ ) is not necessarily same as  $\phi_1$ . As the Infrared band light curves have larger phase gaps and  $\phi_1$  depends on the value of  $t_0$ , we expect a greater scatter in these bands as observed in Fig. 7 and 8. For example, in Fig. 1 the  $J$ -band light curve for *T MON* show a flatter maxima, which also causes an uncertainty in the determination of exact phase corresponding to maximum light. The phase

difference at maximum light for Cepheids in the Galaxy in multiple bands is discussed in Madore & Freedman (1991) while  $\Delta\phi_{max}(I \text{ vs. } JHK_s)$  for first results of LMC Cepheids used in our analysis is discussed in Macri et al. (2014). This phase difference at maximum light and its variation with wavelength is related to Period-Color relations at maximum light discussed in Bhardwaj et al. (2014).

We also emphasize that the coefficients  $\phi_i$  are not independent of time translation and this is the reason phase parameters ( $\phi_{i1}$ ) are preferred to study the light curve structure (Simon & Lee 1981). These are perhaps more easily compared between data sets where the initial epoch of observation is not known. The variation of phase parameters with period and wavelength will be discussed in the following subsections.

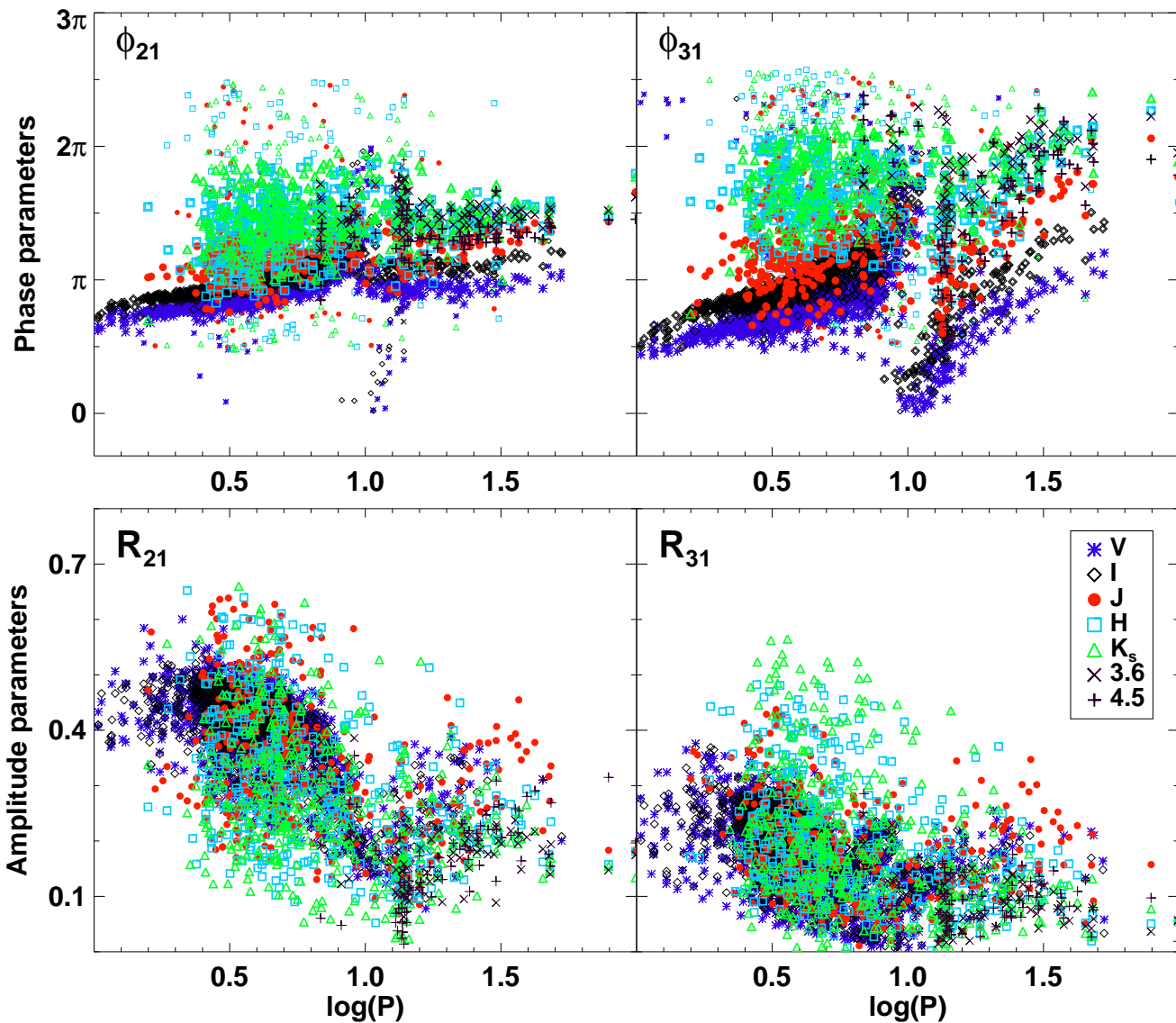


Figure 10. Same as Fig. 9, but for LMC Cepheids.

## 5.2 Individual Fourier Parameters

In order to analyze the variation of Fourier parameters as a function of wavelength and period, we over-plotted the phase and amplitude parameters using different symbols and colors for each band, and removed  $2\sigma$  outliers to make the Hertzsprung progressions more easily visible. Figs. 9 and 10 present the parameters for the Galactic and LMC samples, respectively.

We observed a clear trend in the  $\phi_{21}$  &  $\phi_{31}$  for both Galactic and LMC Cepheids that become larger with increasing wavelength at fixed period. For these phase parameters the outliers are shown using smaller symbols for all bands to avoid any loss of features near the center of the HP. These outliers follow the same trend as all points and the features of the plot are not affected by varying the degree of outlier removal. No clear trend with wavelength at fixed period is seen for the  $R_{21}$  and  $R_{31}$ . Considering long-period

( $\log(P) > 1.0$ ) variables, the amplitude parameters can be separated into two groups; one for  $VIJ$  and another for the longer wavelengths. Furthermore, the latter bands exhibit a slight drop after  $\log(P) = 1.3$  ( $P = 20$  d) while the former ones seem to rise. We also observed a turnover in amplitude parameters around  $\log(P) = 1.5$  that varies with wavelength. Since we have removed  $2\sigma$  outliers in this Figure, the Galactic data show more clearly that the center of the Hertzsprung progression occurs slightly before  $\log(P) = 1.0$  for all parameters while it remains at  $\log(P) = 1.0$  for the LMC variables.

## 5.3 Mean Fourier Parameters

In order to clearly discern any wavelength dependent variation in Fourier parameters, we computed sliding mean values with steps of 0.04 dex in  $\log(P)$  and a bin width of 0.2 dex.



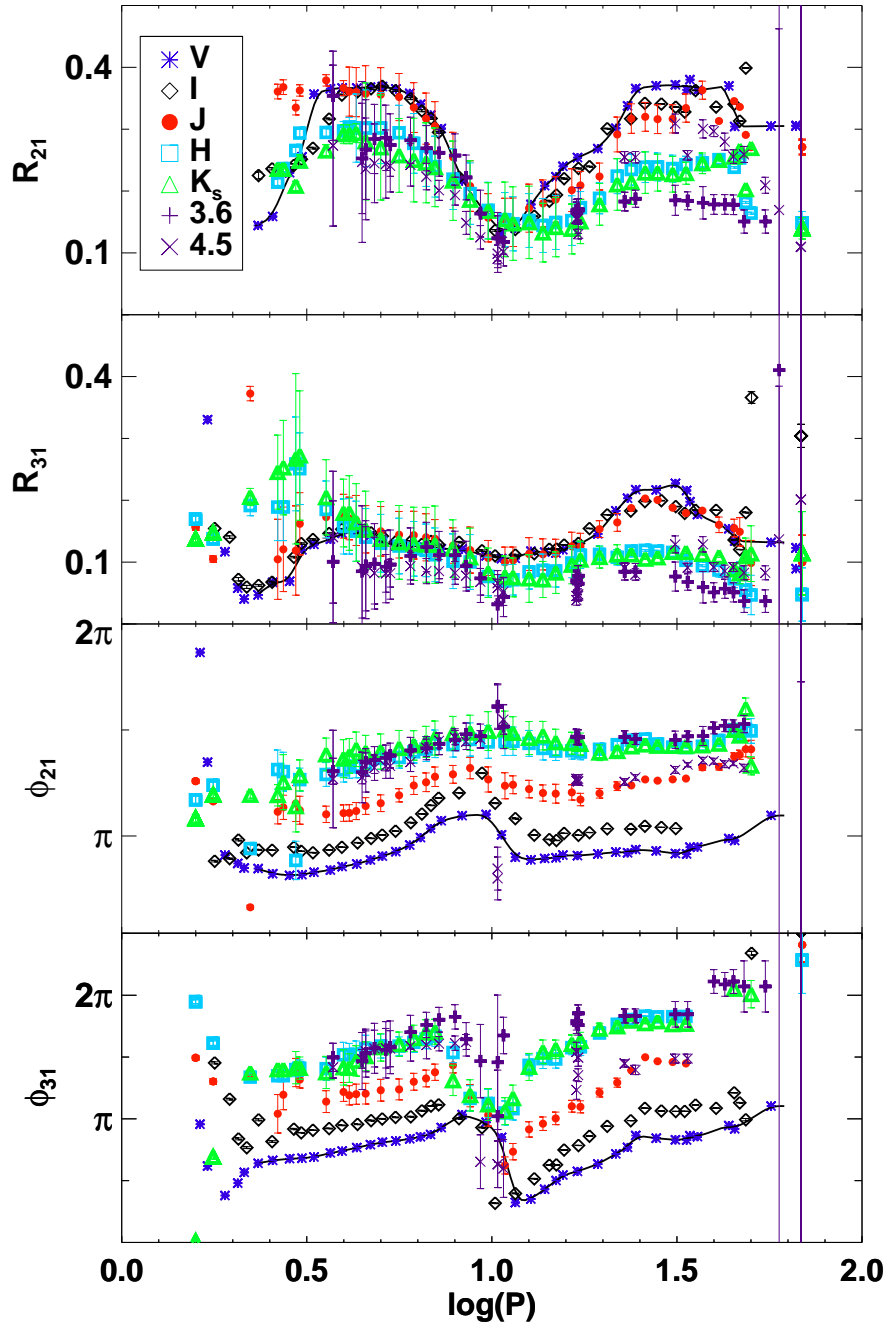


**Figure 11.** Mean Fourier Parameters for Galactic Cepheids. Some phase parameters have been shifted by  $2\pi$  for plotting purposes. The error bars represent the standard error in the mean values.

We found these values yielded the least amount of scatter between consecutive points after significant experimentation with various choices.

Fig. 11 shows the result for Galactic Cepheids. The increase in phase parameters with increasing wavelength becomes more clear and distinct. We also see clearly the decrease in amplitude parameters with increasing wavelength at a given period. Both  $R_{21}$  &  $R_{31}$  exhibit a sharp rise beyond  $\log(P) = 0.9$  to a peak around  $\log(P) = 1.4$  and

a decrease around  $\log(P) = 1.7$ . This behavior is more pronounced for  $VIJ$  than for the redder bands. The minimum is more pronounced for  $R_{21}$ , while  $R_{31}$  shows a shallower minimum. There is also a hint of change in the behavior of the parameters for  $\log(P) > 1.8$ . This may be connected to the properties of ultra long period Cepheids (ULPCs, Ngeow et al. 2013). Considering the short-period variables, both parameters exhibit maximum values around  $\log(P) = 0.6$ . The increased scatter for  $\log(P) < 0.5$  may



**Table 4.** Variation of mean Fourier parameters, determined as a difference in multiple-bands in each period bin of  $\log(P) = 0.2$ .

$\log(P)$	$\Delta R_{21}(V, I)$	$\Delta R_{21}(V, K_s)$	$\Delta R_{21}(J, K_s)$	$\Delta R_{21}(H, K_s)$	$\Delta R_{21}(3.6, K_s)$	$\Delta R_{21}(3.6, 4.5)$
Galaxy						
0.5-0.7	0.031±0.002	0.082±0.064	0.081±0.076	0.018±0.081	0.020±0.097	0.047±0.149
0.7-0.9	0.005±0.002	0.101±0.059	0.071±0.070	0.016±0.073	0.033±0.070	0.045±0.051
0.9-1.1	-0.003±0.001	-0.001±0.040	0.002±0.053	0.003±0.057	0.004±0.054	0.042±0.043
1.1-1.3	0.023±0.001	0.080±0.034	0.047±0.041	0.011±0.042	0.020±0.038	0.018±0.020
1.3-1.5	0.022±0.000	0.127±0.002	0.090±0.002	0.012±0.002	-0.038±0.015	-0.084±0.018
LMC						
0.5-0.7	0.001±0.005	0.105±0.108	0.066±0.124	0.032±0.130	-0.318±0.108	0.000±0.000
0.7-0.9	0.007±0.005	0.058±0.098	0.047±0.121	0.003±0.120	0.002±0.191	-0.066±0.356
0.9-1.1	0.003±0.004	-0.057±0.080	0.032±0.104	0.021±0.105	-0.004±0.145	-0.015±0.170
1.1-1.3	0.026±0.003	0.060±0.063	0.029±0.078	0.011±0.081	-0.039±0.074	0.038±0.055
1.3-1.5	0.044±0.003	0.163±0.046	0.099±0.061	0.016±0.059	-0.022±0.049	-0.008±0.028
$\log(P)$	$\Delta R_{31}(V, I)$	$\Delta R_{31}(V, K_s)$	$\Delta R_{31}(J, K_s)$	$\Delta R_{31}(H, K_s)$	$\Delta R_{31}(3.6, K_s)$	$\Delta R_{31}(3.6, 4.5)$
Galaxy						
0.5-0.7	-0.006±0.001	-0.028±0.061	-0.005±0.072	-0.016±0.076	-0.074±0.097	-0.012±0.125
0.7-0.9	-0.007±0.002	-0.002±0.060	0.011±0.071	-0.012±0.074	-0.021±0.075	0.021±0.051
0.9-1.1	-0.007±0.001	0.025±0.040	0.022±0.049	-0.006±0.051	-0.021±0.057	-0.003±0.046
1.1-1.3	-0.005±0.001	0.034±0.031	0.035±0.039	0.007±0.040	-0.017±0.035	0.027±0.018
1.3-1.5	0.020±0.000	0.099±0.002	0.078±0.002	0.005±0.002	-0.028±0.013	-0.015±0.016
LMC						
0.5-0.7	-0.001±0.005	-0.022±0.104	-0.021±0.119	0.012±0.130	-0.215±0.104	0.000±0.000
0.7-0.9	0.003±0.005	-0.061±0.090	-0.038±0.111	-0.001±0.117	0.034±0.210	-0.010±0.292
0.9-1.1	-0.000±0.004	-0.037±0.085	-0.038±0.108	-0.002±0.112	-0.040±0.152	0.015±0.177
1.1-1.3	0.006±0.003	0.050±0.064	0.034±0.080	0.015±0.083	-0.039±0.075	-0.026±0.055
1.3-1.5	0.031±0.003	0.141±0.042	0.089±0.057	0.024±0.056	-0.010±0.046	0.008±0.028
$\log(P)$	$\Delta \phi_{21}(V, I)$	$\Delta \phi_{21}(V, K_s)$	$\Delta \phi_{21}(J, K_s)$	$\Delta \phi_{21}(H, K_s)$	$\Delta \phi_{21}(3.6, K_s)$	$\Delta \phi_{21}(3.6, 4.5)$
Galaxy						
0.5-0.7	-0.303±0.005	-1.673±0.257	-0.836±0.285	-0.192±0.310	-0.203±0.321	0.115±0.422
0.7-0.9	-0.331±0.006	-1.460±0.250	-0.614±0.283	-0.118±0.311	-0.145±0.310	0.080±0.232
0.9-1.1	-0.499±0.009	-1.466±0.274	-0.709±0.331	-0.140±0.366	0.098±0.427	0.827±0.392
1.1-1.3	-0.308±0.004	-1.691±0.194	-0.753±0.228	-0.096±0.239	0.083±0.225	0.639±0.129
1.3-1.5	-0.354±0.002	-1.554±0.007	-0.524±0.009	0.057±0.010	0.128±0.092	0.586±0.104
LMC						
0.5-0.7	-0.356±0.014	-1.679±0.412	-0.843±0.450	-0.231±0.495	-4.434±0.412	0.000±0.000
0.7-0.9	-0.350±0.017	-1.329±0.353	-0.600±0.423	-0.169±0.465	0.175±0.963	0.658±1.120
0.9-1.1	-0.399±0.023	-1.346±0.398	-0.608±0.472	-0.138±0.494	-0.070±0.672	0.092±0.863
1.1-1.3	-0.495±0.016	-1.665±0.399	-0.711±0.478	-0.088±0.510	0.193±0.495	0.531±0.532
1.3-1.5	-0.498±0.010	-1.592±0.207	-0.518±0.257	-0.026±0.269	0.031±0.232	0.505±0.151
$\log(P)$	$\Delta \phi_{31}(V, I)$	$\Delta \phi_{31}(V, K_s)$	$\Delta \phi_{31}(J, K_s)$	$\Delta \phi_{31}(H, K_s)$	$\Delta \phi_{31}(3.6, K_s)$	$\Delta \phi_{31}(3.6, 4.5)$
Galaxy						
0.5-0.7	-0.634±0.010	-2.251±0.386	-0.823±0.467	0.193±0.501	0.169±0.722	0.082±0.669
0.7-0.9	-0.621±0.013	-2.321±0.329	-0.812±0.392	0.057±0.417	0.272±0.540	0.293±0.574
0.9-1.1	0.418±0.012	-1.065±0.396	-0.753±0.486	-0.091±0.512	1.197±1.012	1.747±1.104
1.1-1.3	-0.591±0.007	-3.377±0.235	-1.673±0.284	-0.121±0.329	0.704±0.330	1.197±0.321
1.3-1.5	-0.700±0.002	-3.042±0.012	-1.104±0.014	0.116±0.017	0.198±0.178	1.229±0.211
LMC						
0.5-0.7	-0.633±0.027	-1.834±0.680	-0.557±0.787	0.018±0.826	-4.311±0.679	0.000±0.000
0.7-0.9	-0.678±0.032	-1.425±0.587	-0.151±0.760	0.363±0.776	0.390±1.410	3.220±1.748
0.9-1.1	-0.175±0.036	-1.023±0.609	0.047±0.782	0.521±0.785	-0.579±1.298	0.892±1.699
1.1-1.3	-0.791±0.022	-2.490±0.592	-0.687±0.720	0.457±0.781	0.951±0.852	1.561±0.772
1.3-1.5	-0.819±0.015	-1.691±0.381	0.304±0.447	0.640±0.504	0.392±0.444	-0.318±0.342

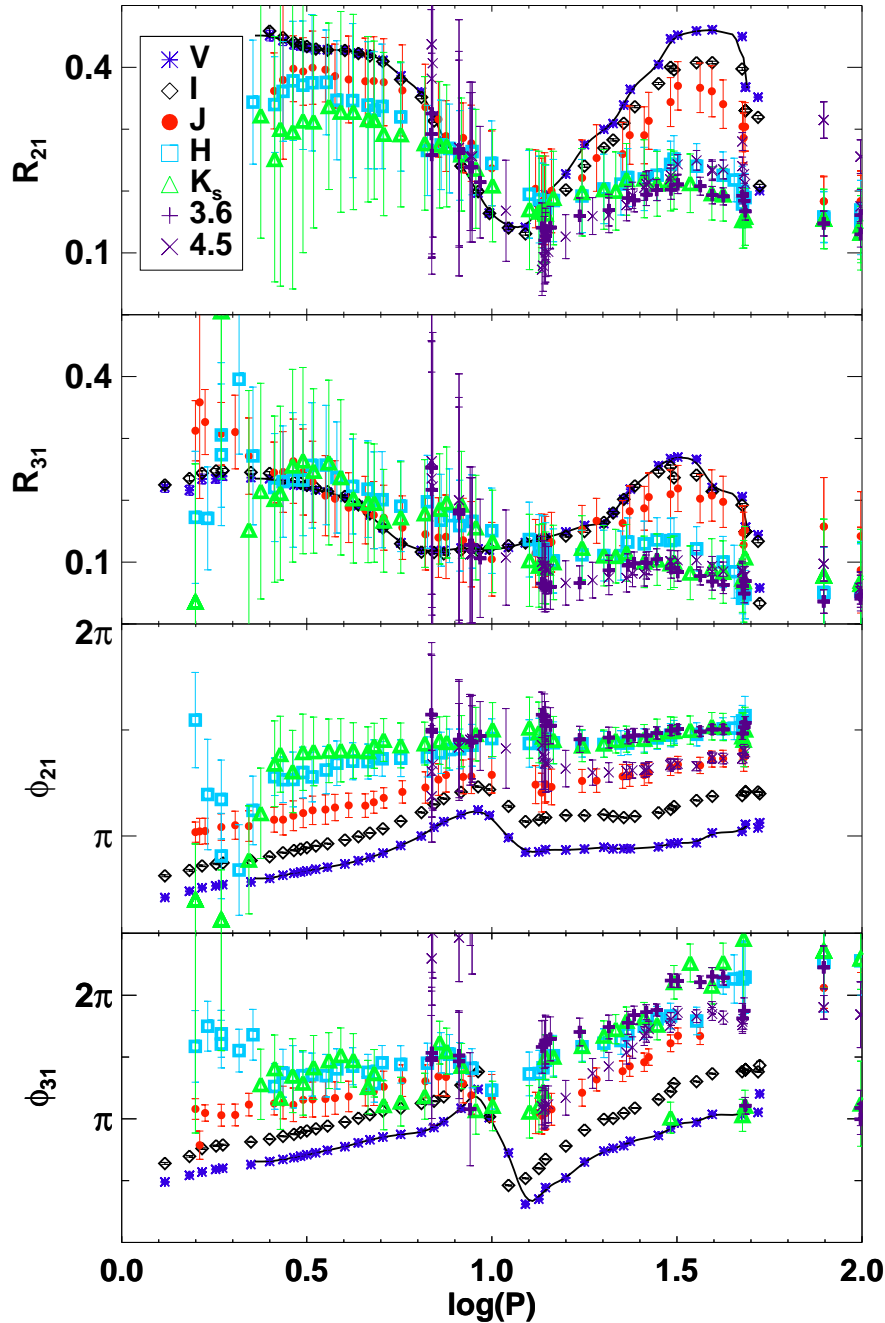


Figure 12. Same as Fig. 12, but for LMC Cepheids.

be due to a combination of a smaller number of stars and contamination by first overtone pulsators.

The corresponding plots for LMC Cepheids are presented in Fig. 12. The same patterns present in Galactic Cepheids are also seen in this sample. The data suggest a separation between optical and infrared Fourier phase parameters for  $\log(P) < 0.5$ , which may extend to  $R_{21}$  but is not visible in  $R_{31}$ . Fig. 11 and 12 were used to determine the average behavior of the Fourier parameters with wavelength

at given period. Flat sections in these plots do occur when Fourier parameters oscillate from a high to low value or vice-versa, particularly when we are near the center of the HP. For example, the flat section in  $R_{31}$  for LMC Cepheids in Fig. 12 is due to the  $R_{31}$  clump at periods  $0.8 < \log(P) < 1.0$  observed at optical bands in Fig. 4. However, such plots do provide evidence that the Hertzsprung progression is most dramatic at shorter wavelengths and in  $R_{21}$  and  $\phi_{21}$  parameters (Simon & Lee 1981).

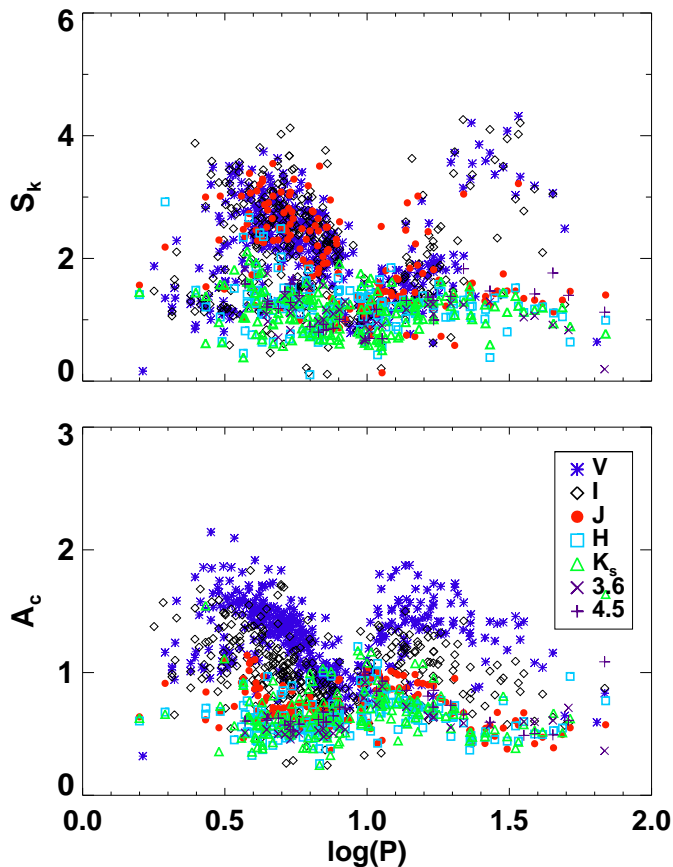


Figure 13. Variation of skewness ( $S_k$ ) and acuteness ( $A_c$ ) parameter against  $\log(P)$  for Galactic Cepheids.

We quantitatively analyzed the progression of mean Fourier parameters with period and wavelength by calculating the change in mean parameter values (binned every 0.2 dex in  $\log(P)$ ) across two bands. We restricted the analysis to  $0.5 < \log(P) < 1.5$  because this period range provides smooth progressions for each parameter with reduced scatter. The result of this analysis is given in Table 4, for both the Galaxy and LMC. Comparing the  $V$ - and  $I$ -band results, we observed a negligible change in amplitude parameters while there was a nearly constant offset in phase parameters for all period bins except for the one centered at  $\log(P) = 1.0$ . Comparing the optical to near-infrared results, the change in amplitude parameters is small around  $\log(P) = 1.0$ , increasing slowly up to  $\log(P) = 1.3$  and sharply afterwards. The change in the values of amplitude parameters when comparing wavelengths shorter and longer than  $J$  is greatest for  $1.3 < \log(P) < 1.5$ . In case of the phase parameters, we observed a similar and significant difference in most of the periods bins. The comparisons of  $H$  to  $K_s$  and  $3.6$  to  $4.5\text{-}\mu\text{m}$  exhibit a small change in amplitude parameters and a large scatter in the phase parameters. We note that  $\Delta\phi$  values for  $(V, K_s)$ ,  $(J, K_s)$ ,  $(H, K_s)$  increase as a function of wavelength, while  $\Delta R$  values decrease as a function of wavelength for  $0.5 < \log(P) < 1.5$ .

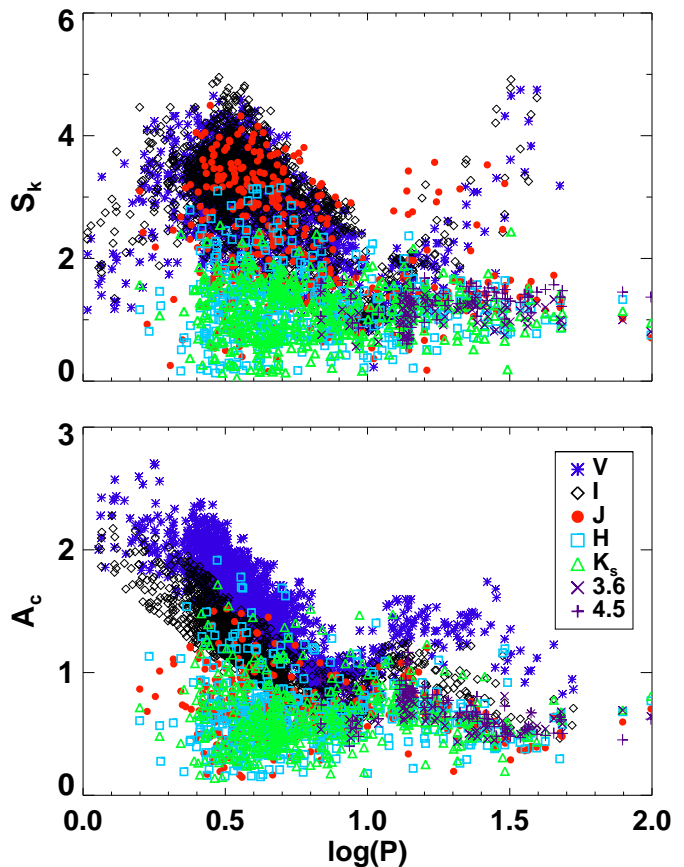


Figure 14. Same as Fig. 13, but for LMC Cepheids.

#### 5.4 Skewness and acuteness parameters

We also observed the variation of skewness ( $S_k$ ) and acuteness ( $A_c$ ) parameters following the work of Stellingwerf & Donohoe (1986, 1987) and Bono, Marconi & Stellingwerf (2000). Stellingwerf & Donohoe (1987) defined skewness as the ratio of the phase duration of the descending branch to the phase duration of the rising branch. They defined acuteness as the ratio of the phase duration during which the magnitude is fainter than the median magnitude to the phase duration during which it is brighter than median magnitude. If  $\phi_{min}$  and  $\phi_{max}$  are the phases corresponding to the extremum of the rising branch, the phase duration of the rising branch is  $\phi_{rb} = \phi_{max} - \phi_{min}$ . Similarly, following Bono, Marconi & Stellingwerf (2000), we defined the median magnitude to be,  $m_{med} = 0.5 \times (m_{max} + m_{min})$  and  $\phi_{fw}$  as the full width at half maximum of the light curve, which is equivalent to phase duration of brighter than average light. Hence

$$S_k = \frac{1}{\phi_{rb}} - 1; \quad A_c = \frac{1}{\phi_{fw}} - 1.$$

The skewness is a measure of left/right asymmetry and it decreases when the slope of the rising branch becomes flatter while acuteness is a measure of the top-

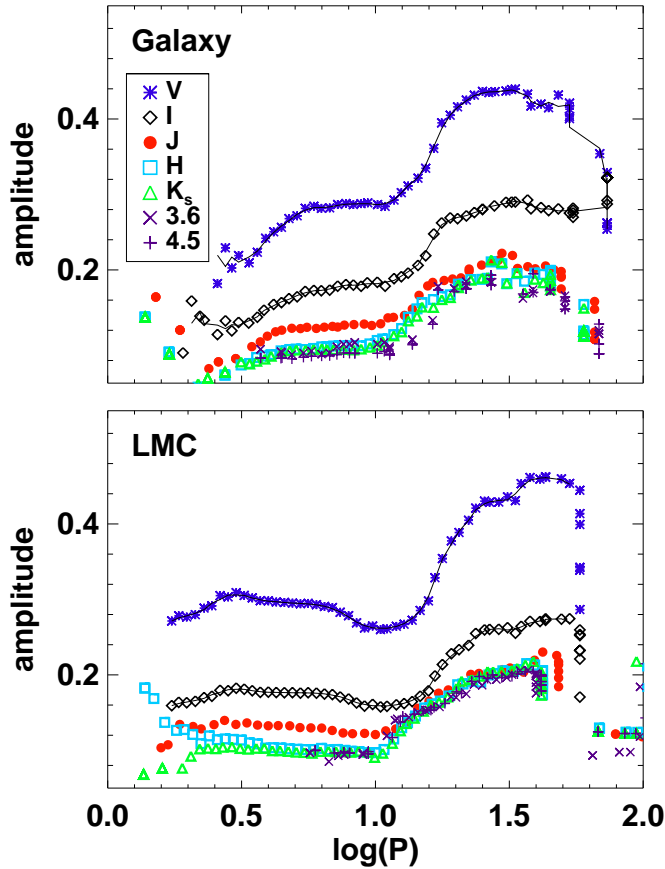


**Figure 15.** Variation of the mean of light curve amplitudes in multiple bands with period for Galactic and LMC Cepheids.

down asymmetry of the light curve and it decreases when the shape changes from sawtooth to flat-topped (Bono, Marconi & Stellingwerf 2000). For observed stars, the  $S_k$  is generally greater than unity while for symmetric light curves both parameters attain a value close to 1. Since, both skewness and acuteness parameters are a function of phase durations, we use equation 2 to obtain 1000 data points per light curve to determine an accurate value of  $\phi_{rb}$  and  $\phi_{fw}$ . The variation of  $S_k$  and  $A_c$  with period and wavelength is shown in Fig. 13 and 14 for the Galaxy and LMC, respectively. At a fixed period, we find that the value of  $S_k$  and  $A_c$  decreases with wavelength. Also, the separation in the values of both parameters for wavelengths shorter/longer than  $J$ -band is clearly visible for Cepheids having  $\log(P) > 1.3$ . This behavior is similar to that of mean Fourier parameters discussed in the previous subsection. As the light curves from optical to infrared bands become more sinusoidal and flat-topped, both the parameters are generally expected to decrease with wavelength. However, the Cepheids having period in the vicinity of 10 days are more symmetric as both parameters attain a value close to unity. We emphasize that the skewness/acuteness parameters are the functions of light curve shape similar to Fourier parameters so either set can be used to see the variation as they are not independent of each other.

## 6 THE VARIATION OF THE HERTZSPRUNG PROGRESSION WITH WAVELENGTH

We also observed the variation of mean of light curve amplitudes with period and wavelength. We apply sliding mean calculations to determine the mean amplitudes similar to mean Fourier parameters. The variation of mean amplitudes at multiple bands for both Galactic and LMC Cepheids is shown in Fig. 15. The mean amplitudes decrease with increasing wavelengths. The amplitudes in the optical bands show a sharp rise for periods  $1.0 < \log(P) < 1.5$  as compared to infrared bands.

The mean parameter plots for both Galactic and LMC Cepheids provide evidence for clearly visible trends that could be fit using functional forms. We therefore reduced the step size in the sliding mean calculation to 0.02 in  $\log(P)$  with the same bin width of  $\log(P) = 0.2$  and fit polynomials of varying degrees. These were then interpolated to obtain values every 0.01 dex. We have presented the functional fit to  $V$ -band parameters in Figs. 11, 12 & 15. We also provide functional fits to multiple band Fourier amplitude parameter ( $R_{21}$ ) and Fourier phase parameter ( $\phi_{21}$ ). These plots will be used to determine the central period of HP, and are shown in Figs. 16 & 17. Similar functional fits were also applied to light curve amplitudes and  $\phi_{31}$  parameter to determine central period of HP.

Following the work of Bono, Marconi & Stellingwerf (2000), we determine the central period of HP using light curve amplitudes. However, we do not observe a sharp minima around  $\log(P) = 1.0$  but we also note that both theoretical light and velocity curve display a flatter minima in Bono, Marconi & Stellingwerf (2000). The variation of the central period of the HP determined using the light curve amplitudes is presented in the top panel of Fig. 18. For optical wavelengths, we find that the central period of the HP is at  $\log(P) = 1.04$  for  $V$ -band and  $\log(P) = 1.03$  for  $I$ -band, in the LMC. These results are in good agreement with the theoretical prediction of  $\log(P) = 1.051 \pm 0.018$  by Bono, Marconi & Stellingwerf (2000).

We determined the minimum values of  $R_{21}$  as a function of wavelength for each sample - these are given in the second panel of Fig. 18. The results argue for a clear trend in the central period of the HP, with the central value increasing with wavelength. For Galactic data at wavelengths longer than  $K_s$ , the central period of the HP shifts toward shorter periods. The increased scatter at mid-infrared wavelengths is expected as there are not enough stars in those bands, specially in the vicinity of 10 days. We find that the central period of HP is at  $\log(P) = 1.05$  for  $V$ -band and  $\log(P) = 1.06$  for  $I$ -band, in the LMC. Again, these results are in excellent agreement with those predicted using theoretical light curves (Bono, Marconi & Stellingwerf 2000) & obtained using Fourier parameters (Welch et al. 1997). However, we emphasize that the results of Bono, Marconi & Stellingwerf (2000) are obtained using the amplitudes of light and velocity curves while our results are obtained using Fourier amplitude parameter. So the central period of HP determined using the two methods are different but the agreement in these two results is very interesting. We do not plot the corresponding values for  $R_{31}$  since the data imply that this parameter seems to be less sensitive to the bump progression and a shallow minimum is observed in Fig. 12.

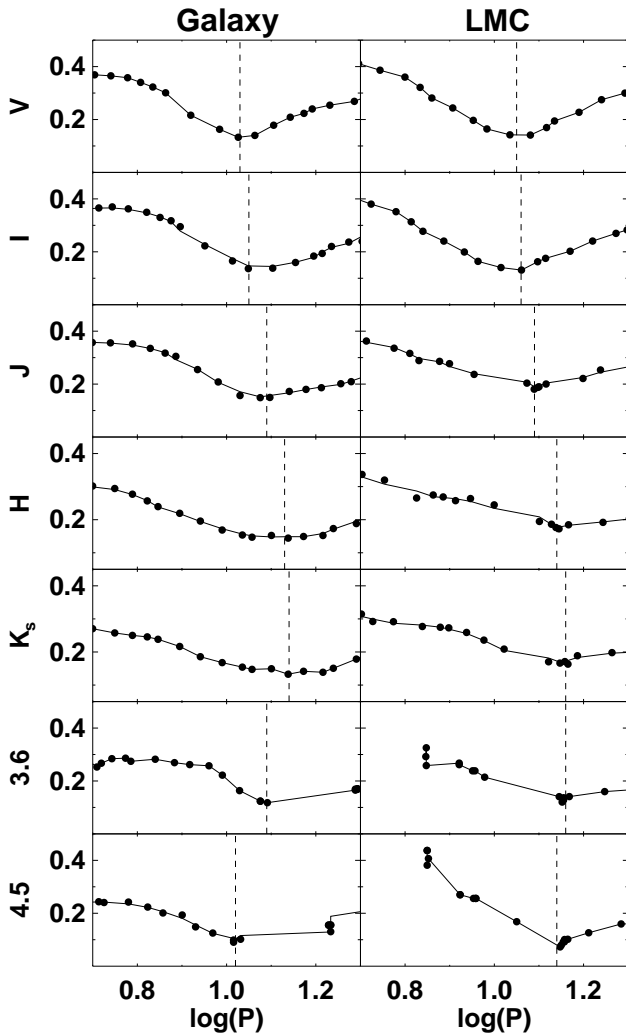


**Figure 16.** Functional fits to mean Fourier amplitude parameter ( $R_{21}$ ) in multiple-bands, used to determine the central period of HP. The dashed vertical line represents the central period of HP in each band. Similarly, functional fits were also applied to mean light curve amplitudes to obtain the center of HP.

In the case of phase parameters, the break in the center of the HP required a slightly different approach. We fit two polynomials to the points on each side of  $\log(P) = 1.0$ , restricting the range to  $\pm 0.2$  dex from that value. We then estimated the maximum value before 10 days and the minimum value just after 10 days. We linearly interpolated across these extrema and took the mid-point of the resulting line to be the center of the HP. We do not observe sharp minima after 10 days at infrared bands due to smaller amplitudes and larger scatter in phase parameters, as shown in Fig. 17. However, there is a small but significant drop in the value of  $\phi_{21}$  in the vicinity of 10 days. In such cases, where the minima is flat or extended towards a longer period, we have chosen the first point lying on the functional fit as minima after 10 days. We consider the mid point of these extremums obtained from functional fits as the center of HP. The re-

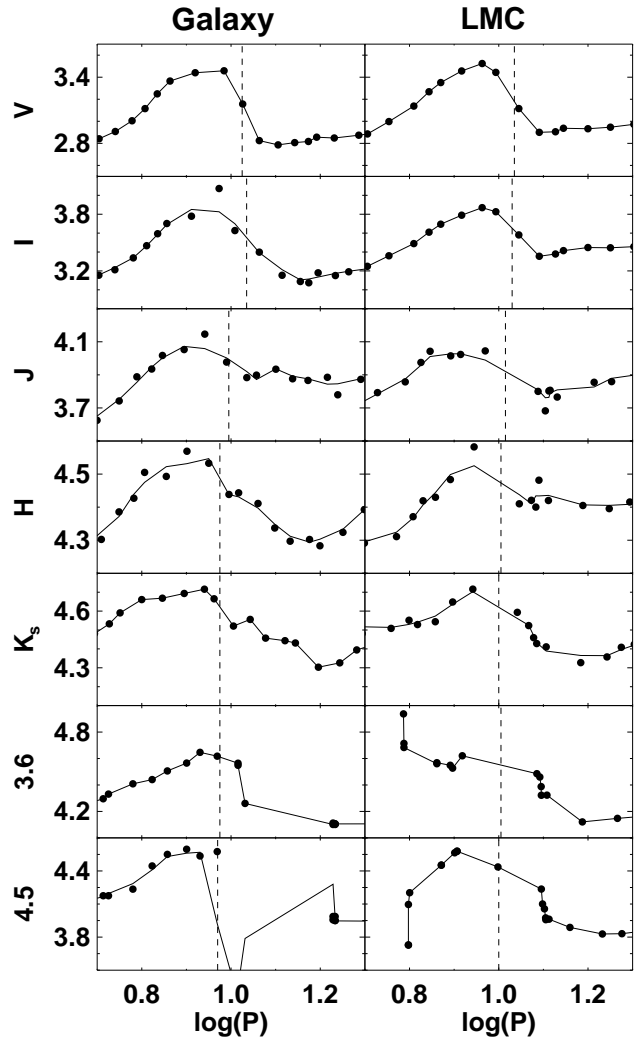


**Figure 17.** Functional fits to mean Fourier phase parameter ( $\phi_{21}$ ) in multiple-bands, used to determine the central period of HP. The dashed vertical line represents the central period of HP in each band. Similarly, functional fits were also applied to  $\phi_{31}$  to obtain the center of HP.

sults obtained from the fits to phase parameters are shown in the bottom two panels of Fig. 18. Again, there seems to be a clear trend in the value of the center of the HP, but now decreasing with increasing wavelength. In case of  $\phi_{21}$ , the central period occurs at  $\log(P) \sim 1.04$  in the optical bands for both Galaxy and LMC, consistent with the previous determination of  $\log(P) = 1.049 \pm 0.031$  by Welch et al. (1997).

We have also observed a slight difference in the central period of the HP for the Galaxy and LMC in each parameter. This difference is most likely due to metallicity differences between the two galaxies. As seen in Fig. 18, the greatest disparity in the central period of the HP happens longwards of  $K_s$  for amplitude &  $R_{21}$  and beyond  $J$  for  $\phi_{21}$ . No significant difference is seen for  $\phi_{31}$ . Since we have obtained these results using the sliding mean calculations, it is difficult to determine the exact significance of these re-



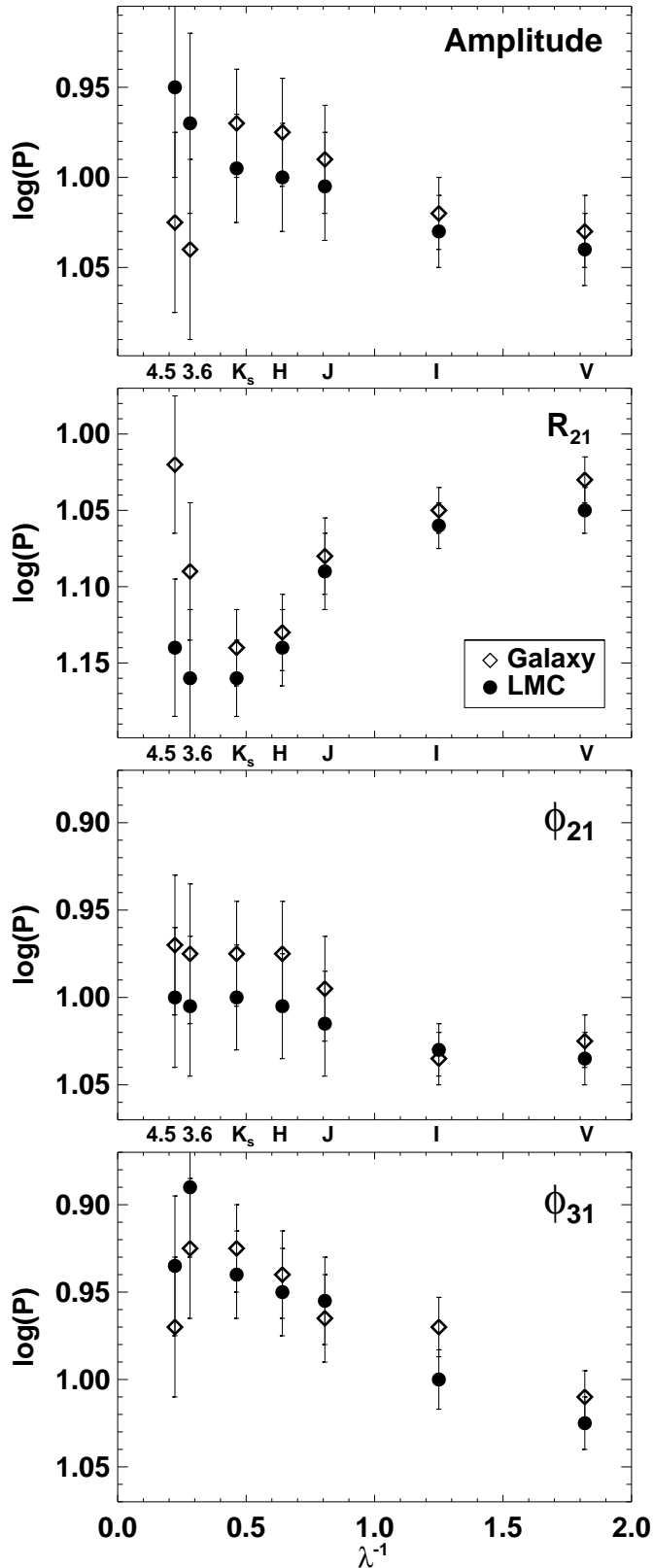


Figure 18. Variation of central period of HP with wavelength for amplitude and Fourier parameters  $R_{21}$ ,  $\phi_{21}$  &  $\phi_{31}$ . The error bars represent the maximum possible deviation from the median value with different degree of polynomials.

sults specially at longer wavelengths, where the number of stars is smaller in the vicinity of  $\log(P) = 1.0$ . Since we applied the same procedure at all bands, there is a differential effect in these parameters that seems to be real. Also, this confirms the work of Beaulieu (1998), who has determined the center of the HP for our Galaxy, LMC and SMC Cepheids using Fourier parameters. Beaulieu (1998) found a shift in the HP center towards the longer periods for the Galaxy having lower mean metallicity, following the work of Andreasen & Petersen (1987); Andreasen (1988). However, we emphasize that more data will be needed to determine the central period more accurately, particularly at longer wavelengths.

## 7 CONCLUSIONS

In the present study, we discussed the Fourier decomposition of Galactic and LMC Cepheid light curves in multiple bands. We compiled and made use of the largest data sets available in each band. We analyzed the variation of Fourier parameters in detail to observe some interesting patterns. We found an increase in phase parameters with increasing wavelength for both Galactic and LMC variables. We also observed a decrease in amplitude parameters with increasing wavelength. An interesting pattern in amplitude parameters was observed, which suggests that for  $VIJ$ -band, the amplitude parameters increases sharply as compared to longer wavelengths for periods greater than around 20 days. Quantitatively this was summarized by determining the difference of mean Fourier parameters in multiple bands. We also observed a decrease in skewness and acuteness parameters as function of wavelength at a fixed period suggesting Cepheid light curves to be more symmetric at longer wavelengths.

The central period of the HP displays a clear variation with increasing wavelength, suggesting an increase in central period for Fourier amplitude parameters and a decrease for phase parameters. At optical bands, the mean central period of the HP occurs at  $\log(P) \sim 1.03$  for the Galaxy and at  $\log(P) \sim 1.04$  for the LMC, which are consistent with the previous studies (Welch et al. 1997; Bono, Marconi & Stellingwerf 2000). We also found small differences in the central period of the HP for different Fourier parameters between the Galaxy and LMC. These differences are mainly in the  $R_{21}$  beyond  $K_s$  and in  $\phi_{21}$  beyond  $J$ . These differences are such that Galactic data have the central period at shorter values. At optical bands, this difference is more accurate and confirms previous work by Beaulieu (1998) but we can not determine the exact significance at infrared bands due to larger scatter in amplitude and phase parameters.

We also observed a flatter variation in  $R_{31}$  amplitude parameter as compared to other Fourier parameters in the vicinity of 10 days. This shallower minimum is more pronounced in the mean Fourier parameters shown in Fig. 11 and Fig. 12. Further, we observed a clump in the  $R_{31}$  in the vicinity of  $0.7 < \log(P) < 1.0$  for  $VI$ -bands (see Fig. 4), which is a possible cause of flatter minimum in Fig. 12. However, this clump is not visible for Galactic Cepheids because of the smaller number of stars as compared to OGLE LMC data. We investigated the light curves of stars in/out side the clump but with similar periods. Examples are shown in



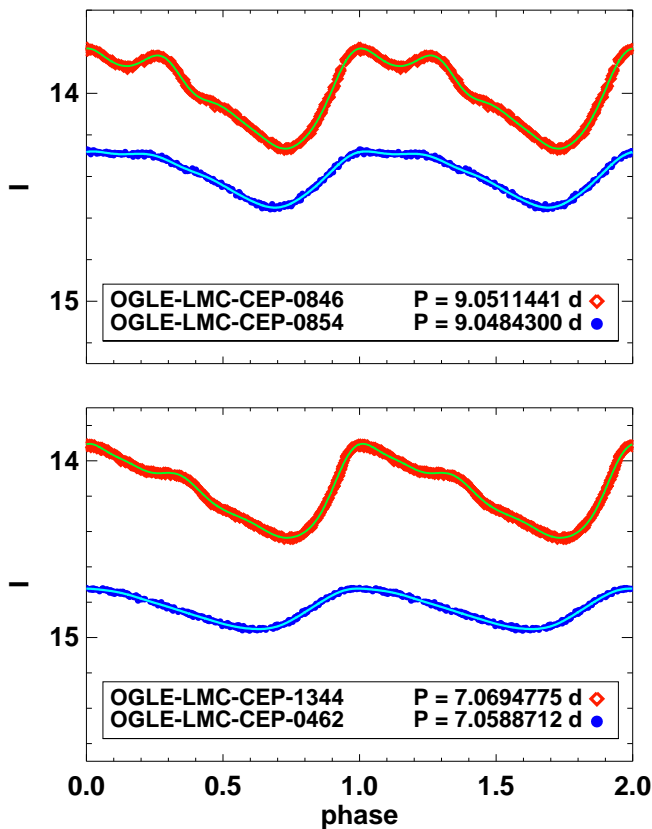


**Figure 19.** Examples of I-band light curves of LMC Cepheids, which have periods in the vicinity of clump in  $R_{31}$  parameters in Fig. 4. Light curves in red/blue color are from in/out side of the clump respectively.

Fig. 19. A slight bump after the maximum light (minimum magnitude) is observed in the light curves for the stars that are in the clump noted in the  $R_{31}$  vs.  $\log(P)$  plot (Fig. 4). This feature will be extensively studied in a future work and may provide a direct link between light curve structure and Fourier parameters.

The variation of Fourier parameters with wavelength can shed light on pulsation physics that are wavelength dependent. Further, these results can serve as a benchmark to constrain theoretical stellar pulsation models that now routinely incorporate model stellar atmospheres and produce light curves at various wavelengths.

While a physical interpretation of Fourier parameters is still an open question, the method does provide a quantitative description of the structure of Cepheid and RR Lyrae light curves. In order to have more confidence in these models, it will be important to compare these model and observed light curves, quantitatively with Fourier parameters as a function of metallicity, wavelength and period.

## ACKNOWLEDGMENTS

AB is thankful to the Council of Scientific and Industrial Research, New Delhi, for a Junior Research Fellowship (JRF)

and to Sukanta Deb for helpful discussions. This work is supported by the grant provided by Indo-U.S. Science and Technology Forum under the Joint Center for Analysis of Variable Star Data. CCN thanks the funding from Ministry of Science and Technology (Taiwan) under the contract NSC101-2112-M-008-017-MY3. LMM acknowledges support by the United States National Science Foundation through AST grant number 1211603 and by Texas A&M University through a faculty start-up fund and the Mitchell-Heep-Munnerlyn Endowed Career Enhancement Professorship in Physics or Astronomy. We also thank the anonymous referee for his/her useful suggestions that improved the quality of the paper. This research was supported by the Munich Institute for Astro- and Particle Physics (MIAPP) of the DFG cluster of excellence “Origin and Structure of the Universe”. This work has made use of NASA’s Astrophysics Data System, SIMBAD database and the VizieR catalogue, McMaster Cepheid Photometry database and the data products from the Two Micron All Sky Survey.

## REFERENCES

- Andreasen G. K., 1988, *A&A*, 196, 159  
 Andreasen G. K., Petersen J. O., 1987, *A&A*, 180, 129  
 Antonello E., Poretti E., 1986, *A&A*, 169, 149  
 Baart M. L., 1982, *IMA J. Num. Analysis*, 2, 241  
 Barnes, III T. G., Fernley J. A., Frueh M. L., Navas J. G., Moffett T. J., Skillen I., 1997, *PASP*, 109, 645  
 Beaulieu J. P., 1998, *Mem. Soc. Astron. Italiana*, 69, 21  
 Berdnikov L. N., 1987, *Peremennye Zvezdy*, 22, 530  
 Berdnikov L. N., 1992, *Soviet Astronomy Letters*, 18, 130  
 Berdnikov L. N., 2008, *VizieR Online Data Catalog*, 2285, 0  
 Berdnikov L. N., Ignatova V. V., Pastukhova E. N., 1998, *Astronomical and Astrophysical Transactions*, 15, 81  
 Berdnikov L. N., Turner D. G., 2001, *Astronomical and Astrophysical Transactions*, 19, 689  
 Berdnikov L. N., Turner D. G., 2004a, *Astronomical and Astrophysical Transactions*, 23, 395  
 Berdnikov L. N., Turner D. G., 2004b, *Astronomical and Astrophysical Transactions*, 23, 599  
 Berdnikov L. N., Vozyakova O. V., 1995, *Astronomy Letters*, 21, 308  
 Berdnikov L. N., Yakubov S. D., 1993, *Peremennye Zvezdy*, 23, 47  
 Bhardwaj A., Kanbur S. M., Singh H. P., Ngeow C.-C., 2014, *MNRAS*, 445, 2655  
 Bono G., Marconi M., Stellingwerf R. F., 2000, *A&A*, 360, 245  
 Deb S., Singh H. P., 2009, *A&A*, 507, 1729  
 Deb S., Singh H. P., 2010, *MNRAS*, 402, 691  
 Deb S., Singh H. P., 2014, *MNRAS*, 438, 2440  
 Fernie J. D., Evans N. R., Beattie B., Seager S., 1995, *Information Bulletin on Variable Stars*, 4148, 1  
 Jurcsik J., Kovacs G., 1996, *A&A*, 312, 111  
 Kovacs G., Shlosman I., Buchler J. R., 1986, *ApJ*, 307, 593  
 Laney C. D., Stobie R. S., 1992, *A&A*, 93, 93  
 Leavitt H. S., Pickering E. C., 1912, *Harvard College Observatory Circular*, 173, 1  
 Macri L. M., Ngeow C.-C., Kanbur S. M., Mahzooni S., Smitka M. T., 2014, *ArXiv e-prints*, 1412.1511

- Madore B. F., Freedman W. L., 1991, *PASP*, 103, 933
- Monson A. J., Freedman W. L., Madore B. F., Persson S. E., Scowcroft V., Seibert M., Rigby J. R., 2012, *ApJ*, 759, 146
- Monson A. J., Pierce M. J., 2011, *ApJ*, 193, 12
- Moskalik P., Buchler J. R., Marom A., 1992, *ApJ*, 385, 685
- Nemec J. M. et al., 2011, *MNRAS*, 417, 1022
- Ngeow C.-C., Kanbur S. M., Nikolaev S., Tanvir N. R., Hendry M. A., 2003, *ApJ*, 586, 959
- Ngeow C.-C., Lucchini S., Kanbur S., Barrett B., Lin B., 2013, *ArXiv e-prints*, 1309.4297
- Persson S. E., Madore B. F., Krzemiński W., Freedman W. L., Roth M., Murphy D. C., 2004, *AJ*, 128, 2239
- Poretti E., 1994, *A&A*, 285, 524
- Scowcroft V., Freedman W. L., Madore B. F., Monson A. J., Persson S. E., Seibert M., Rigby J. R., Sturch L., 2011, *ApJ*, 743, 76
- Simon N. R., 1977, *ApJ*, 217, 160
- Simon N. R., 1985, *ApJ*, 299, 723
- Simon N. R., 1986, *ApJ*, 311, 305
- Simon N. R., 1988, in *Astrophysics and Space Science Library*, Vol. 148, *Pulsation and Mass Loss in Stars*, Stalio R., Willson L. A., eds., p. 27
- Simon N. R., Davis C. G., 1983, *ApJ*, 266, 787
- Simon N. R., Kanbur S. M., 1995, *ApJ*, 451, 703
- Simon N. R., Lee A. S., 1981, *ApJ*, 248, 291
- Simon N. R., Moffett T. J., 1985, *PASP*, 97, 1078
- Simon N. R., Schmidt E. G., 1976, *ApJ*, 205, 162
- Simon N. R., Teays T. J., 1982, *ApJ*, 261, 586
- Soszynski I. et al., 2008, *Acta Astronomica*, 58, 163
- Stellingwerf R. F., Donohoe M., 1986, *ApJ*, 306, 183
- Stellingwerf R. F., Donohoe M., 1987, *ApJ*, 314, 252
- Stetson P. B., 1996, *PASP*, 108, 851
- Ulaczyk K. et al., 2013, *Acta Astronomica*, 63, 159
- Welch D. L. et al., 1997, in *Variables Stars and the Astrophysical Returns of the Microlensing Surveys*, Ferlet R., Maillard J.-P., Raban B., eds., p. 205
- Welch D. L., Wieland F., McAlary C. W., McGonegal R., Madore B. F., McLaren R. A., Neugebauer G., 1984, *ApJs*, 54, 547